POLITECNICO
MILANO 1863

SCUOLA DI INGEGNERIA INDUSTRIALE
E DELL'INFORMAZIONE

Automatic detection tool for abdominal aortic aneurysm

Tesi di Laurea Magistrale in
Mathematical Engineering - Ingegneria Matematica

Author: **Bruno Viti**

Student ID: 965651
Advisor: Prof. Luca Formaggia
Co-advisors: Luca Azzolin, Abele Simona
Academic Year: 2021-22

Abstract

In this work, we want to develop an automatic detection tool for abdominal aortic aneurysm (AAA). Abdominal aortic aneurysm is a vascular pathology with a high mortality rate and consists of a local enlargement of the abdominal aorta called aneurysm. The aneurysm is formed by two components, the lumen, which is the passageway through which blood flows, and the thrombus, a blood clot surrounding the lumen. In many cases, the aneurysm grows too much and the only way to proceed is surgery.
Doctors require quantitative information about the aneurysm both for diagnosis and presurgical planning. This type of information can be obtained by analyzing, manually, the scans taken from medical imaging, i.e. X-rays, Magnetic Resonance Imaging (MRI), or Computed Tomography (CT). The automatic detection tool aims to accelerate and automatize the manual procedure, in order to give to doctors useful information concerning the aneurysm. In this new tool, the quantitative analysis of the scans is performed through image segmentation.
Image segmentation is the process of simplifying an image by extracting only the contents of our interest. In our case, we want to extract, from the medical images, the lumen and the thrombus and, to do that, we have to choose the criterion of extraction. We first detect the lumen, relying on its geometry, then we face the thrombus's detection, formulating and solving a minimization problem through morphological operators. At the end of the segmentation, we are also able to compute quantitative indicators which, together with the reconstruction of the aneurysm, can help doctors in their decisions.

Keywords: Abdominal aortic aneurysm, medical imaging, image segmentation, morphological operators.

Abstract in lingua italiana

In questo lavoro, si vuole sviluppare uno strumento di identificazione automatica per un aunerisma addominale aortico (AAA). Un aneurisma addominale aortico è una patologia vascolare con un alto tasso di mortalità e consiste in un rigonfiamento dell'aorta addominale chiamato aneurisma. L'aunerisma è costituito da due componenti, il lumen, attraverso il quale scorre il sangue, e il trombo, un coagulo di sangue che circonda il lumen. In molti casi, l'aneurisma cresce troppo e l'unica soluzione è un intervento chirurgico.
I dottori necessitano di informazioni quantitative riguardanti l'aneursima sia per la diagnosi che per la pianificazione chirurgica. Questo tipo di informazioni può essere ottenuto analizzando, manualmente, scansioni di immagini mediche, come raggi X, Risonanze Magnetiche, o Tomografie Computerizzate (TC). Lo strumento di identificazione automatica vuole accelerare e automatizzare la procedura manuale, per consegnare ai dottori informazioni utili in merito all'aunerisma. In questo nuovo strumento, l'analisi quantitativa delle scansioni è compiuta attraverso segmentazione di immagini.
La segmentazione di immagini è un processo per semplificare un immagine estraendo solo il contenuto di nostro interesse. Nel nostro caso, vogliamo estrarre dalle immagini mediche il lumen e il trombo e, per farlo, dobbiamo stabilire un criterio di riconoscimento. Come prima cosa identifichiamo il lumen, basandoci sulla sua geometria, successivamente affrontiamo il problema del trombo, formulando e risolvendo un problema di minimizzazione attraverso opeatori morfologici. Alla fine della segmentazione, saremo in grado anche di calcolare indicatori quantitativi che, insieme alla ricostruzione dell'aunerisma, possono aiutare i dottori nelle loro decisioni.

Parole chiave: Aneurisma addominale aortico, immagini mediche, segmentazione di immagini, operatori morfologici.

Contents

Introduction

Abdominal aortic aneurysm (AAA) is a vascular disease associated with a high rate of mortality, and it consists of a local enlargement of the abdominal aorta called aneurysm. The aneurysm is formed by two components, the lumen, which is the passageway through which blood flows, and the thrombus, a blood clot surrounding the lumen. The enlargement is considered an aneurysm if the diameter is greater than 3 cm or more than 50% larger than normal. The more the aneurysm grows, the more the risk of rupture increases and, if grows too much, the only curative way is a surgical approach.
For doctors, having information about the aneurysm is of the utmost importance. These information could be the dimension of the thrombus or its position around the aorta, and they could help the doctors with the diagnosis but, more important, with the presurgical planning. In order to have the necessary data, doctors need a view of the patient's anatomy and to obtain that they resort to medical imaging.
Medical imaging is the technique of imaging the interior of the body, and it could be performed in many ways, the most used procedures are X-rays, Magnetic Resonance Imaging (MRI), and Computed Tomography (CT). The output of these methods is a set of images (scans), which display the patient's anatomy. A quantitative analysis of that scans is the key to reconstructing the structures of interest and getting quantitative indicators such as lengths and volumes. In our framework, we want to use the scans of a patient to reconstruct the lumen, and the thrombus, and then proceed to compute the most useful measurements of the detected volumes. This procedure of scan analysis can be performed manually, by an expert surgeon, or automatically, employing image segmentation. Image segmentation is a process to simplify an image, extracting the information of our interest. This technique is exploited in many frameworks, in our case, it could be used to extract the aorta and the aneurysm from the inputs given by medical imaging.
In this thesis, we have developed an automatic detection tool for abdominal aortic aneurysm, which takes in input the patients' scan, and automatically performs a quantitative study of the pathology, giving as output the thrombus' 3D reconstruction together with meaningful indicators.
In Chapter 1, we show how image segmentation works and how we can exploit it for

medical purposes and, in particular, to cope with AAA. In Chapter 2, we go through the implementation of the algorithm, discussing the choices that we made and the methods that we decided to use. We start by describing the detection methods for the aorta and the thrombus. In the first case, we exploit the geometry of the aorta to detect correctly the artery. For the thrombus, instead, we formulate the segmentation problem as a minimization problem, and we solve the PDEs that follow through morphological operators. Then we address the problems of calcifications, which are accumulations of salts. Finally, we examine different indicators, which can be computed from the reconstruction and can be used by doctors. In Chapter 3, we show the 3D reconstruction of the structure previously detected, and we comment on the indicators that have been computed. In Chapter 4 we review the algorithm and we explore possible extensions.

1 | Image segmentation and its application to abdominal aortic aneurysm

In this chapter, we give an overview of the main techniques of image segmentation, focusing on their application in medical imaging and, in particular, in the detection of the abdominal aortic aneurysm (AAA).

1.1. Image segmentation

An image is a way of transferring information, and it contains lots of useful data. Images can be represented as 2D (or 3D) matrices, where each element, called pixel, constitute a color at a single point in the image. There are different types of images, one of the most common are the gray-scale type.
Gray-scale images, or black-and-white images, consist of singular-value pixels corresponding to the gray level of the image. These gray levels span the full range from black to white in a series of very fine steps, normally 256 different grays. In particular, the value 0 corresponds to a black pixel, while 255 corresponds to a white pixel.

Figure 1.1: Gray-scale range

Since each pixel contains a single value, a 2D image can be represented by a 2D matrix I, such that $I \in P^{w \times l}$, where $P = [0, 255]$, while w and l are the dimension of the image. There exist other types of images, but for medical application gray-scale image are the most common choice.

Sometimes, we are interested in specific components of the image, and consequently, we need to consider only part of the information. Image segmentation is a method by which we can extract, from an image, the part of the information we are interested in. In particular, the goal of segmentation is to simplify and/or change the representation of an image into something more meaningful and easier to analyze.
There are plenty of fields in which segmentation plays an important role, such as medical image processing, face recognition, and autonomous driving. In our case, image segmentation could be helpful to reconstruct the geometry of the aorta and the aneurysm, from which the doctor will extract useful information.
Up to now, many different algorithms for image segmentation have been developed, summarized in the following section.

1.1.1. Region-based Segmentation

The simplest segmentation technique is the Region-based Segmentation that is divided into two subclass: Threshold Segmentation and Regional Growth Segmentation.

Threshold Segmentation

Threshold segmentation is the most common algorithm since it is fast and easy to implement. It can only be used on gray-scale images and takes into account only the intensity value of the pixel. The drawback is that it is difficult to obtain accurate results where there is no significant gray scale difference in the image.
The simplest implementation is binary segmentation, in which if a pixel has a higher intensity than a fixed threshold belongs to set A, otherwise belongs to set B. There are also more sophisticated variants. For example, in [1], a more advanced technique based on threshold segmentation is developed.

Regional Growth Segmentation

The basic idea of regional growth method is to have pixels with similar properties together to form a region. The method requires first selecting a seed pixel and then merging the similar pixels around the seed pixel into the region where the seed pixel is located.
The advantage of regional growth is that it usually separates the connected regions with the same characteristics and provides good boundary information and segmentation results. The disadvantage is that the computational cost is large. Also, the noise and grayscale unevenness can lead to voids and over-division. In [2] a regional growth algorithm is applied in medical imaging to detect brain disease in MRI.

1.1.2. Edge Detection Segmentation

The edge of the object constitutes a discontinuous local feature of the image, which could be a change in local brightness, such as color mutation, texture changes, and so on. The use of discontinuities to detect the edge is the basis of Edge Detection Segmentation.
In an image, there are many discontinuities between adjacent pixels and it is difficult to identify them as edges. An edge can often be detected using derivative operations, in particular, we can compute the gradients of the pixels' intensity and detect the edges as the regions of a high gradient. This type of segmentation can be exploited in medical imaging, in [3] an improved edge detection algorithm is developed for brain tumor.

1.1.3. Clustering Segmentation

A cluster is a collection of objects which are "similar" among themselves and are "dissimilar" to the objects belonging to other clusters. Clustering methods include soft clustering (e.g., Fuzzy c-means or FCM) and hard clustering (e.g., fuzzy k-means or FKM).
In hard clustering, each data point is clustered or grouped into one cluster. Each data point, may either completely belong to a cluster or not. The k-means clustering algorithm clusters data by iteratively computing the mean intensity for each class and segmenting the image by classifying each pixel in the class with the closest mean.
In soft clustering, instead of inserting each data point into separate clusters, the algorithm assigns to each pixel a probability of belonging to a certain cluster. In soft clustering or fuzzy clustering, each data point can belong to multiple clusters along with its probability score or likelihood. Fuzzy c-means algorithm generalizes the k–means algorithm allowing soft clustering. In [4] an alternative Kernelized FCM algorithm (KFCM) that could improve MRI segmentation is presented.

1.1.4. Active Contour technique ("Snakes")

Active contours, or snakes, are one of the most widely used computer vision tools. Recent results have shown that they can achieve robust detection performance, and this task is formulated in variational terms, where an image induces an energy functional on a curve or surface. Minimizing the functional in a steepest descent manner evolves the surface towards a local minimum that represents the solution of the problem.
Two examples of this approach are the Geodesic Active Contour (GAC) and the Active Contours Without Edges (ACWE) algorithms. In the GAC, the energy functional is a geodesic in a Riemannian manifold with a metric induced by image features, in its simplest case the target borders. The ACWE does not need well-defined borders, and it is

less sensitive to the initial configuration and the model parameters.
Both approaches are based on the level-set formulation. The curve is evolved by propagating an interface represented by the zero level-set of a smooth function, using a time-dependent PDE. The resolution of the latter is computationally costly, and in the case of the simplest finite-difference explicit numerical scheme, it has stability constraints on the size of the time step. A review of these methods is presented in [5] and it involves morphological operators.

Morphological Active Contour technique

Monotone contrast-invariant and translation-invariant operators are called morphological operators. The idea developed in [5] is to find a relation between differential and morphological operators, in particular the authors show that the composition of different morphological operators approximates the numerical solution of PDEs.
In section (2.1.3), we discuss a more exhaustive analysis of these operators, focusing on their application in medical image segmentation.

1.2. Medical image segmentation for AAA

Image segmentation is widely used for medical purposes, as we have seen in the previous sections. The automatic detection of features helps doctors in many aspects as diagnosis or surgical planning. This is true also for pathology concerning the aorta, and in particular, for the Abdominal Aortic Aneurysm (AAA).

1.2.1. The pathology

The aorta is the main and largest artery in the human body, originating from the left ventricle of the heart and extending down to the abdomen, where it splits into two smaller arteries, the iliac arteries. The aorta distributes oxygenated blood to all parts of the body through the systemic circulation.
In anatomical sources, the aorta is usually divided into sections. The thoracic aorta runs from the heart to the diaphragm, and the abdominal aorta, from the diaphragm to the iliac bifurcation. The abdominal aorta travels down the posterior wall of the abdomen, anterior to the vertebral column. It thus follows the curvature of the lumbar vertebrae. It runs parallel to the inferior vena cava, which is located just to the right of the abdominal aorta, and becomes smaller in diameter as it gives off branches [6].
Abdominal aortic aneurysm (AAA) is a localized enlargement, aneurysm, of the abdominal aorta, a vascular disease with a high mortality rate. Usually, the swelling consists

of two components, the lumen, which is the channel through which blood flows, and the thrombus, a blood clot surrounding the lumen. In some patients, calcifications, i.e. accumulations of calcium, form on the artery's wall and constitute another important component of the aneurysm.
The enlargement is considered an AAA if the diameter of the aorta is greater than 3 cm or more than 50% larger than normal. They cause no symptoms but the rupture of the aneurysm often leds to the death of the patient. In those with an aneurysm less than 5.5 cm, the risk of rupture in the next year is below 1%, while among those with an aneurysm between 5.5 and 7 cm, the risk is about 10%. Finally for those with an aneurysm greater than 7 cm the risk is about 33%. The mortality if ruptured is 85% to 90%.
AAAs occur most commonly in those over 50 years old, in men, and among those with a family history. In particular, AAAs affect 2-8% of males over the age of 65. The most common risk factors are smoking, high blood pressure, and other blood diseases [7].
There exist two types of AAA, saccular and fusiform. In this thesis, we consider only patients with a fusiform aneurysm.

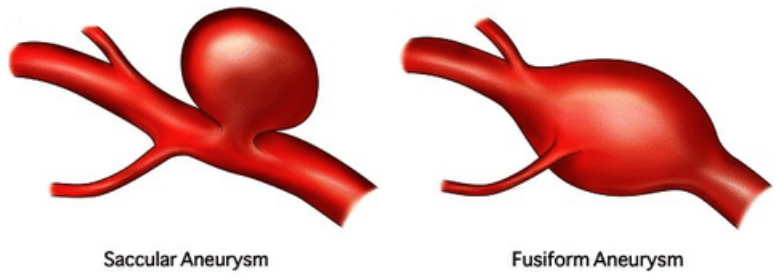

Figure 1.2: Types of aneurysm

To prevent this disease, the most common recommendations are abstinence from smoking, avoiding overweight and treating high blood pressure and high blood cholesterol. If the prevention does not work a surgical treatment is needed.

Current guidelines suggest that if the AAA grows too much, over 5.5 cm in males and over 5 cm in females, or if the maximal transversal diameter grows by more than 5 mm in a year, the only curative treatment is a surgical approach such as open or endovascular surgery. In both methods, a stent graft is used to help keep the aneurysm from bursting, hence previous knowledge of anatomy is extremely useful.
The growth of medical imaging has led to the development of software allowing to create virtual reconstructions of the AAA. The main tool for medical imaging is the quantitative analysis of X-rays scan, contrast-enhanced Computed Tomography Angiography (CTA),

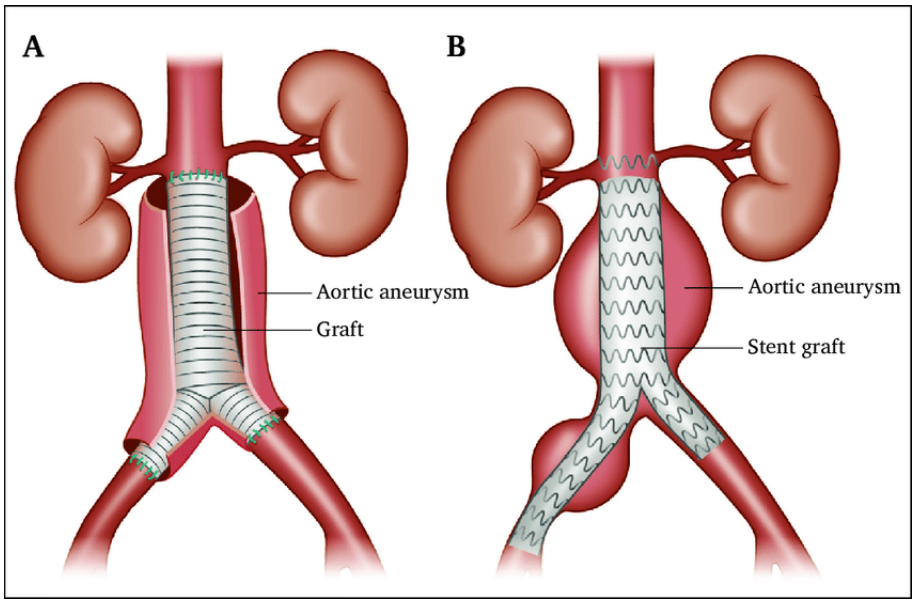

Figure 1.3: (A) Open surgery for an abdominal aortic aneurysm (open AAA repair). The affected segment of the aorta is replaced with a material graft stitched in place. (B) Endovascular AAA repair (EVAR). A stent graft is placed inside the aneurysm to reline the aorta and prevent the aneurysm bursting.[8]

and Magnetic Resonance Imaging (MRI). The latter are essential to assess aortic anatomy, identify the pathology and perform preoperative planning in vascular surgery. All of this information are crucial for the choice of the graft that has to be used in the treatment, hence the detection of the AAA has the utmost importance.

1.2.2. Medical imaging of AAA

The starting point for every detection algorithm is a set of images of the anatomy of the patients. There are three main imaging technologies: X-rays, Computed Tomography scan (CT), and MRI.

X-rays are the most used since they are easy to use, non invasive, and cheap. Even if they have low radiation compared to CT scans they can have side effects, moreover they do not produce high-quality images.

The CT/CTA (CTA are specialized CT for vessels and arteries) is the investigation of choice for evaluating the aorta. Very accurate imaging of the aorta is possible with reasonable doses of iodinated contrast medium, which is handed out to the patient intravenously, but for various purposes, they can also be used intra-arterially. The latter enhances the visibility of vascular structures and organs during radiographic procedures.

CTA accurately shows branch vessel anatomy as well as the configuration of complex

aortic aneurysms and dissections, moreover is the best method for showing calcification in the aortic wall. The best current CT/CTA should have an accuracy approaching 100% in assessing the size of the aorta, detecting dissection, and showing branch vessel anatomy [9]. The drawback of the CT scan is the high quantity of radiation used during the scan. Unlike the previous technologies, MRI has no exposure to radiation. The principal disadvantage is the cost of the operation, which, in addition, can be unpleasant for the duration and the loud noise during it.
In the following, we will focus on CT/CTA and we will consider only data from CT/CTA scan since it is the technology mostly used to detect AAA.

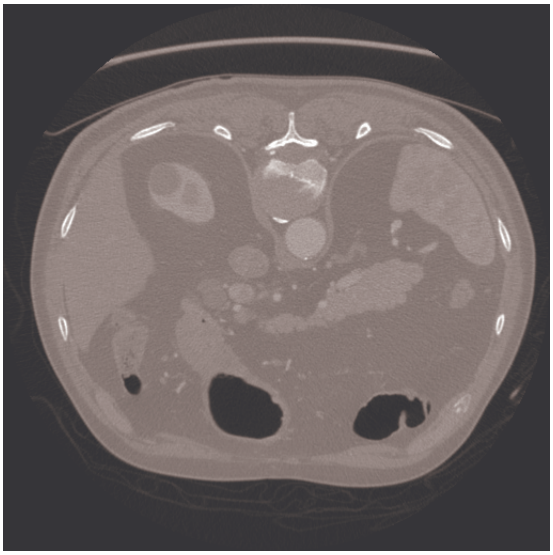

Figure 1.4: Example of CTA scan

1.2.3. The Hounsfield Scale

CT and CTA are images where tissues, bones and organs are characterized by attenuation values. The latter are defined as the radiodensities of each material, which describe the relative inability of radiation to pass through a particular material. Attenuation values are expressed, according to a linear density scale, as "Hounsfield units" (HU), after Sir Godfrey Newbold Hounsfield, the inventor of CT scanning. In the Hounsfield scale, water is arbitrarily assigned a value of 0 HU. All other CT values are computed according to

$$HU = 1000 \cdot \frac{\mu_{tissue} - \mu_{H2O}}{\mu_{H2O}},$$

in which μ is the CT linear attenuation coefficient.
The HU values for each pixel are converted into a digital image by assigning a gray-scale

intensity to each value, the higher the number the brighter the pixel intensity.
Some approximate HU values for tissues commonly found on CT scans are shown in 1.1.

Table 1.1: Hounsfield units for different tissues [10]

Hounsfield units	Tissue
1000	Bone, calcium
100 to 600	Iodinated CT contrast
70	Blood
35	Gray matter
20 to 40	Muscle, soft tissue
0	Water
-30 to -70	Fat
-1000	Air

Looking at the table it is clear why an iodinated medium is used. Increasing the HU value of the blood in the aorta will change the intensity of the pixels corresponding to the lumen, making the detection of the latter easier. Unfortunately, the medium does not affect the thrombus, hence the detection of the blood clot is more challenging.

1.2.4. Automatic tools for image segmentation

The non-automatic segmentation of the aorta could be a time consuming process. An expert vascular surgeon has to identify the lumen of the aorta and the thrombus manually. It is clear that automatising the segmentation could speed up the whole process and, sometimes, it could be even more precise. Moreover, useful physical quantities can be extracted from the segmentation, such as the maximum diameter of the aneurysm, which could decide if a surgical operation is needed.
Currently some semi-automatic and automatic tools has been developed. They mainly divide in two categories:

- Physic based,
- Data based.

In the first case, the segmentation is performed considering the physic of the problem. The shape of the aorta, the width of the aorta, or the intensity of the tissues in the CTAs, are examples of features that are taken into account to identify the lumen.

In the second case a Deep Learning approach is usually exploited. First, a dataset of non-automatic segmentation is provided by experts. Then a Convolutional Neural Network (CNN) is trained and finally, new segmentation can be obtained from the CNN. An example of this type of algorithm for the detection of AAAs is developed in [11].
The main problem of the second approach is the dimension of the training dataset. To guarantee good performances of the CNN, the latter should be trained with a great amount of data, which sometimes can be difficult to obtain.
The first approach, instead, can be implemented independently from the amount of CTAs. For this reason, in this work, a physic based approach is developed.

2 | Workflow for an automatic detection of the aneurysm

In this chapter we will go through the implementation of the algorithm and the choices that have been made during its development. The algorithm has to detect the three main components of the AAA, and is divided in three parts:

- Lumen segmentation,
- Thrombus segmentation,
- Calcifications segmentation.

These steps have to be performed sequentially since each of them is crucial for the next one. In particular, the first step detects the aorta's lumen, whose segmentation is exploited for the second part to correctly detect the thrombus. Finally, in the third and last step, the calcifications surrounding the thrombus and the lumen are segmented.

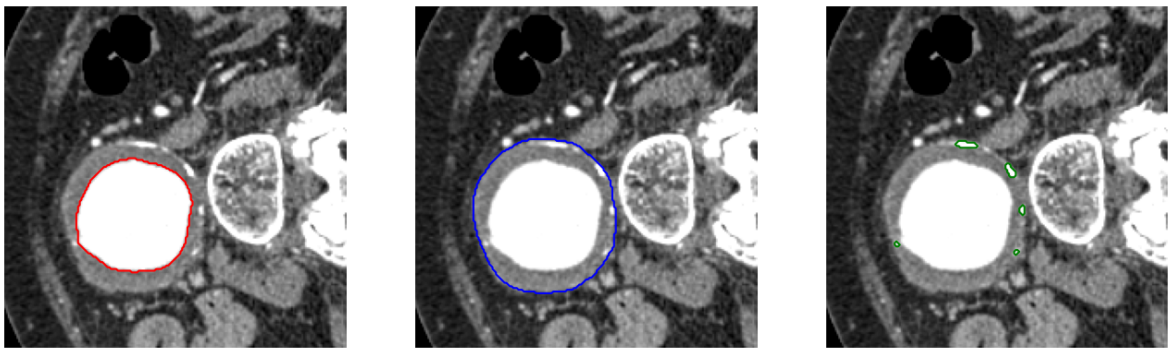

(a) Lumen (b) Thrombus (c) Calcifications

Figure 2.1: View of lumen, thrombus and calcifications. (Patient 4)

2.1. Lumen segmentation

The first step to detect the aneurysm is the identification of the aorta's lumen. In this section, we will see how the segmentation is performed and what is needed before its implementation.

2.1.1. Image pre-processing

Before using any type of algorithm, it is mandatory to perform image pre-processing, to facilitate the detection of the lumen, removing noise and increasing the intensity of the pixels of interest.
The very first thing that we perform is the extraction of a Volume Of Interest (VOI) to reduce the total memory usage and decrease the computational cost. Indeed not all the pixels of the scan are useful for our intent, hence we simply have to crop the CTA slices, as shown in Figure (2.2).
This procedure is fully automatic and does not require the selection of the VOI from the user. We address the implementation of the algorithm in section (2.1.2).

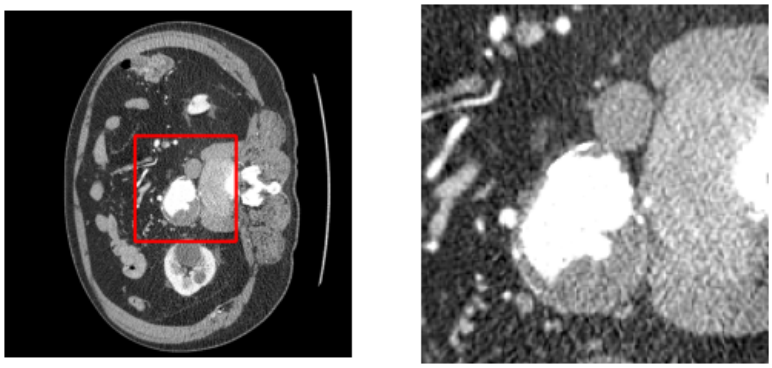

Figure 2.2: (Re-scaled) CTA and (Re-scaled) cropped CTA. (Patient 1)

Second to the cropping, there is the re-sampling. The latter is a standard pre-processing technique in which we change the size of the pixels. In our case, we resize the volume such that the pixels become cubic. The effect of the re-sampling cannot be seen through the image, but it is useful to standardize the image and some algorithms used later could benefit from that.

At this point, we have to enhance the visibility of the lumen. To do that, we re-scale the

scans using the following formula [12]:

$$I = \min\left(255, \max\left(0, \left(H - \left(L - \frac{W}{2}\right)\right) * \frac{255}{W}\right)\right), \tag{2.1}$$

where H is the intensity of the pixels expressed in Hounsfield unit, L is the window level and W is the window width. The window width is the range of the grayscale that can be displayed, while the center of the range is referred to as the window level.
The idea behind this re-scaling is to map the Hounsfield range of intensity into the standard gray-scale range $[0, 255]$. Setting W and L we can evaluate an upper, λ^+ and a lower, λ^- bound such that:

$$I = \begin{cases} 255 & if \quad H \geq \lambda^+, \\ 0 & if \quad H \leq \lambda^-, \\ \left(H - \left(L - \frac{W}{2}\right)\right) * \frac{255}{W} & otherwise, \end{cases}$$

For the lumen's segmentation we used $L = 40$ and $W = 400$, and with these values the bounds are $\lambda^+ = 240\ HU$ and $\lambda^- = -160\ HU$, i.e. all pixels that have an Hounsfield intensity above $240\ HU$ will display in white, the ones below $-160\ HU$ will be black, all the others will take different shape of gray.
We recall that the blood that flows into the aorta has an increased Hunsfield value that goes above λ^+ thanks to the iodinated contrast medium, therefore the lumen is displayed in white.

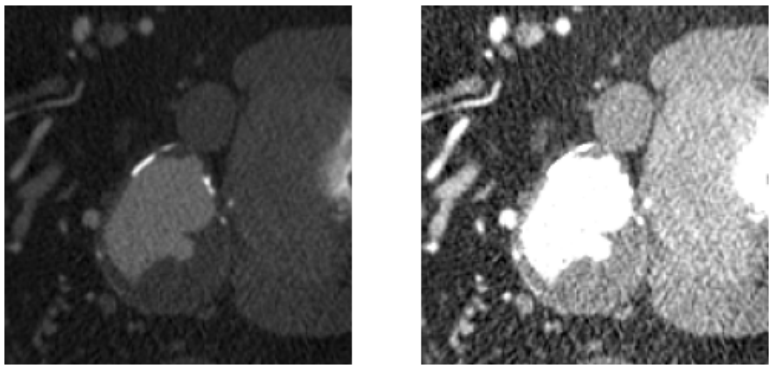

Figure 2.3: Effect of the re-scaling with $L = 40$ and $W = 400$. (Patient 1)

From Figure (2.3) we can easily see the effect of the re-scaling but we can also see that the CTA is affected by noises and it is not homogeneous. Consequently, the difference between

adjacent pixels could be too sharp. The smoothing part is carried out by the `itk` library, in particular, we used the filter `curvature_anisotropic_diffusion_image_filter()`. This filter performs anisotropic diffusion on an image using the modified curvature diffusion equation (MCDE) [13]-[14].

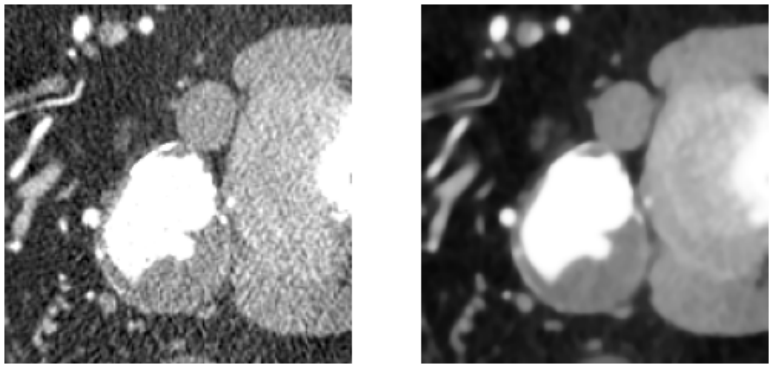

Figure 2.4: CTA before and after the smoothing. (Patient 1)

As we can see from Figure (2.4) the image is now much more homogeneous and is ready for the segmentation algorithm.
We must clarify that all the pre-processing steps are performed not iterating over the slices but directly on the 3D volume. This precaution could be neglected for the re-scaling and the cropping, but it is extremely useful for the smoothing since, in this way, consistency along the z-axis is guaranteed. In the following, unless specifically stated otherwise, we will consider that the algorithms are applied to the 3D volume.

2.1.2. Segmentation

Now we have to extract the segmentation of the lumen from the pre-processed CTA scans. In order to have a first guess we rely on the shape properties of the aorta.
The algorithm consists in iterating over the slices along the z-axis, from the highest to the lowest, and for each of them we perform three steps:

- threshold the slice,
- find the contours,
- select the contours with certain properties.

The technique of thresholding is the most trivial approach for image segmentation. Indeed, it only consists in fixing a threshold ϵ, in this case a value in the range $[0, 255]$, discarding all the pixels with intensity below ϵ and assigning another value, usually 255, to the remaining pixels.

We rely on the library `OpenCv` for this step, exploiting the function `threshold(blur, tr, 255, cv.THRESH_BINARY)`. The input parameters are the scan `blur`, the threshold `tr`, the value to assign to the selected pixel, and the type of thresholding algorithm to use. In our case, the function loops over the pixels of `blur`, and each pixel p is changed to p_{new} performing the following operation

$$p_{new} = \begin{cases} 255 & if \quad p > \texttt{tr}, \\ 0 & otherwise. \end{cases}$$

The output is a binary image according to the threshold.

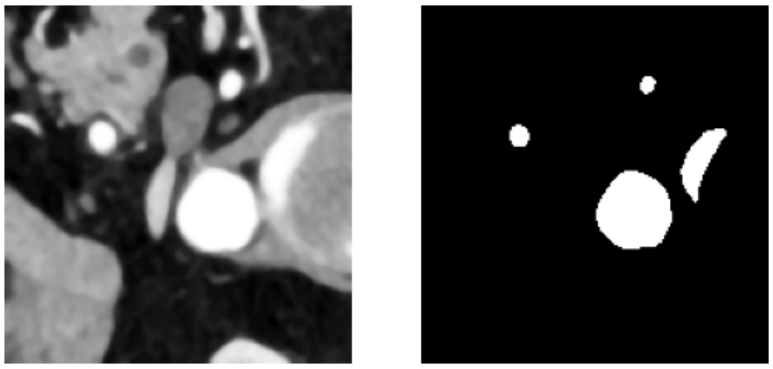

Figure 2.5: CTA before and after the thresholding. (Patient 1)

It is worth showing the result of the thresholding technique applied to the raw CTA instead of the smoothed scan. This comparison helps us to understand the reason behind the smoothing. Without the denoising part, the thresholding collects spurious pixels that in some slices could affect the following steps.

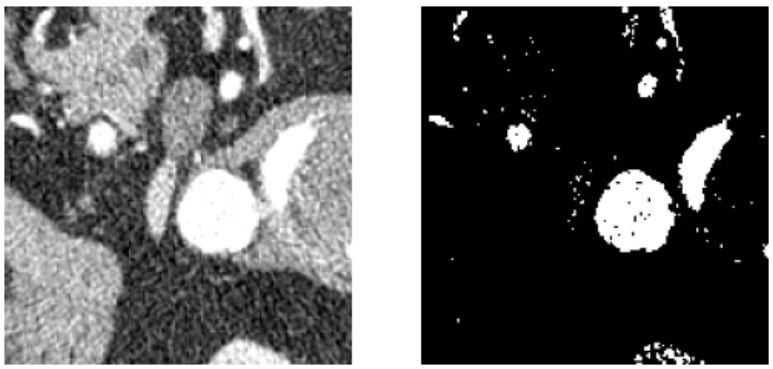

Figure 2.6: Raw CTA before and after the thresholding. (Patient 1)

We use, again, a function from `OpenCv` to find the contours of the output image. The command `findContours(thresh, cv.RETR_TREE, cv.CHAIN_APPROX_SIMPLE)` returns

all the contours of the binary image (`thresh`) given as input. The function detects a pixel p as contour's point if at least one pixel, among its 8 neighborhoods, has value of 0.
The second input of the function is the algorithm to sort the contours, whose implementation is developed in [15]. The last input is the method for storing the contour's points, in our case we do not save all the contour's elements but we compress horizontal, vertical, and diagonal segments saving only their endpoints.

Figure 2.7: Thresholds and corresponding contours. (Patient 1)

For the last step, we need a filter that discards all the contours except the ones of the lumen. In the majority of the slices, the aorta has a regular shape, usually circular. We can exploit this fact to construct our filter.
The properties that we use to discriminate the contours are three geometrical aspects.
The first and most trivial is the *Area*. We can easily find bounds of the lumen's area and discard the contours with area too small or too big. Even if this filter removes for sure some spurious contours, it is not enough.
The second geometrical aspect to consider is the *Solidity*. The latter is defined as:

$$S = \frac{Area}{ConvArea},$$

where $ConvArea$ is the area of the smallest convex set that contains the contour. A value of *Solidity* equal to 1 tells us that the selected contour is convex, if instead the *Solidity* goes towards 0 there is a high probability that the contour is irregular and consequently it has to be discarded.
The last property is the *aspect ratio*, which, again, is defined as a fraction:

$$A = \frac{min(w,h)}{max(w,h)},$$

where w and h are the width and height of the bounding rectangle of the contour. A high

value of *aspect ratio* corresponds to a contour not too elongated in some direction, hence more likely to be a circle. Also in this case we can discard all the contours with values of *aspect ratio* below a fixed value.
We can see from Figure (2.8) that the filter works correctly since only the lumen's contour is kept.

Figure 2.8: Contours before and after the geometrical filter. (Patient 1)

As previously stated, the aorta does not always have a smooth circular shape. Indeed, in the abdomen area, where the thrombus is attached, it could have some irregularities. This problem can be solved by imposing an axial consistency.
Since we are looping over the slices in the z direction, we can add a backup filter if the geometrical one fails. The most natural solution is to impose that the contours in one slice must have an intersection with the previous one, that is spatially collocated above. This trick should cover all the pathological cases that the algorithm could encounter.

After the detection of the aorta's lumen, we still have to refine the segmentation. To cope with that, from now on, morphological snakes will be extensively used. Therefore we give an overview of the mathematical background and the features of these new operators, but before that, we must clarify how the methods described in this section have been used in the cropping part of the pre-processing.

Cropping

Cropping is the first step to perform in order to speed up the algorithm.
We want that the detection tool is fully automatic, therefore each step, including the cropping, should be performed without the user's inputs. To extract the VOI, we need to choose a criterion to determine where the aorta is. We loop through the slices of the original CTAs scans, along the z-axis, and we collect the contours which satisfy certain

geometrical properties. From the first guess of the lumen, we need to extract the bounds of the VOI. Regarding the x and y bounds we simply collect the maximum and minimum coordinates of the lumen's segmentation, and we expand them by a few centimeters in order to contain the aneurysm. The z bounds, instead, are obtained in the following way. The upper bound z_{max} is set to be the last slice which contains the mesenteric artery, a vessel attached to the lumen and easy to detect. The lower bound z_{min} is taken in correspondence to the iliac bifurcation. At this point, we can crop the volume and pass it as input to the lumen segmentation.

2.1.3. Morphological snakes

In this subsection the mathematical formulation of the morphological snakes and their relation with differential operators is discussed in more detail.
Differential operators are fundamental tools in the computer vision and graphics communities. They are key to contour evolution with PDEs, where the infinitesimal change of a contour is given by a differential operator. Let $\mathcal{C} : \mathbb{R}^+ \times [0,1] \rightarrow \mathbb{R}^2$, be a parametrized 2D curve over time. A differential operator L defines the curve evolution with the PDE $\frac{\partial \mathcal{C}}{\partial t} = \mathcal{C}_t = L(\mathcal{C})$. Different forms of L result in different types of evolution. The most trivial is $L(\mathcal{C}) = \mathcal{N}$, where $\mathcal{N}$ is the normal of the curve. With this choice, the curve moves along its normal direction with constant velocity.
Since working with an explicit form of $\mathcal{C}$ is not easy, a level set method has been developed in which the curve is represented implicitly as level set of an embedding function [16]. In other words, $\mathcal{C}(t) = \{(x,y); u(t,(x,y)) = 0\}$, where $u : \mathbb{R}^+ \times \mathbb{R}^2 \rightarrow \mathbb{R}$ is the embedded function. With this representation the curvature equation $\mathcal{C}_t = \mathcal{N}$ becomes

$$\frac{\partial u}{\partial t} = \pm|\nabla u|. \tag{2.2}$$

Another important equation is $\mathcal{C}_t = \mathcal{K}\mathcal{N}$, where $\mathcal{K}$ is the Euclidean curvature of $\mathcal{C}$. The latter in the new formulation becomes

$$\frac{\partial u}{\partial t} = \operatorname{div}\left(\frac{\nabla u}{|\nabla u|}\right) \cdot |\nabla u|. \tag{2.3}$$

Morphological operators are monotone contrast-invariant and translation-invariant operators. The most common ones are the *dilation* and the *erosion* operators. A *dilation* D_h

with radius h of function u is defined as:

$$D_h u(\mathbf{x}) = \sup_{\mathbf{y} \in hB(\mathbf{0},1)} u(\mathbf{x}+\mathbf{y}),$$

while the *erosion* has a similar form:

$$E_h u(\mathbf{x}) = \inf_{\mathbf{y} \in hB(\mathbf{0},1)} u(\mathbf{x}+\mathbf{y}).$$

In both definitions, $B(\mathbf{0}, 1)$ is the ball of radius 1 centered at $\mathbf{0}$ and the term hB is the set B scaled by h, i.e., $hB = \{hx : x \in B\}$.

Some differential operators can be expressed as morphological operators. The key idea of these connections is to study the infinitesimal behaviour of morphological operators. It is has been proved in [17] that:

$$\lim_{h \to 0^+} = \frac{D_h u - u}{h} = |\nabla u|,$$

$$\lim_{h \to 0^+} = \frac{E_h u - u}{h} = -|\nabla u|.$$

This means that the successive application of D_h with very small radius, $\lim_{m\to\infty}(D_{t/m})^m u_0$, is equivalent to the solution of $\frac{\partial u}{\partial t} = |\nabla u|$, with initial value $u(0, \mathbf{x}) = u_0$. A similar argument can be made for E_h.

Thanks to this behaviour, we can approximate the level-set evolution PDE (2.2) using the morphological operators D_h and E_h. In [5] a more advanced curvature morphological operator that approximates (2.3) is introduced, but here we will only focus on the definition of the morphological snakes used for segmentation.

To summarize, we have now a set of morphological operators — *dilation*, *erosion* and the advanced curvature flow operator — which have an infinitesimal behaviour like PDEs (2.2) and (2.3) respectively. These two PDEs are fundamental in many practical applications, since they are part of many contour evolution rules. Thus, given a PDE of contour evolution which includes terms (2.2) and (2.3), we may compose their corresponding morphological operators to approximate the solution. In other words, now we can use mathematical morphology to evolve contours.

Morphological GAC

In the GAC framework, an energy functional, which depends on pixels' intensity I, is assigned to a curve,

$$E(\mathcal{C}) \;=\; \int_0^1 g(I)|\dot{\mathcal{C}}(p)|dp,$$

where $|\dot{\mathcal{C}}(p)|dp$ is the Euclidean arc-length parametrization of the curve, and $g(I) = g(I(\mathcal{C}))$. The term $g(I) : \mathbb{R}^d \to \mathbb{R}^+$ describe the content of the image computing the gradients of pixels' intensity and it allows us to select which regions of the image we are interested in. Tipically it takes the following form:

$$g(I) = \frac{1}{\sqrt{1+\alpha|\nabla(G_\sigma * I)|}},$$

where in this case $G_\sigma *$ is a Gaussian filter with standard deviation σ. This definition of $g(I)$ is low in the edges of the contours, where the gradients of I are steep, hence the functional will attain the minimum along the edges.
The GAC method consists in minimizing the energy functionals in a steepest-descent way, in particular it can be proved that the local minima are reached at the steady states of the differential equation

$$\mathcal{C}_t \;=\; (g(I)\cdot\mathcal{K} \;-\; \nabla g(I)\cdot\mathcal{N})\mathcal{N}.$$

The novelty of the morphological GAC is to rewrite this equation in terms of a level set implementation

$$\frac{\partial u}{\partial t} \;=\; g(I)|\nabla u|\mathrm{div}\left(\frac{\nabla u}{|\nabla u|}\right) \;+\; \nabla g(I)\cdot\nabla u. \tag{2.4}$$

Within the latter expression we recognize PDEs (2.2) and (2.3), which can be solved by means of morphological operators.
In the complete version of the GAC, two additional terms, forces, are added in the PDE. The first one is the *smoothing force*, which tends to smooth the hyper-surface, the second one is the *balloon force*, which inflates or deflates the hyper-surface in areas of low gradient. For the complete description of the problem see [5].

Morphological ACWE

Chan and Vese [18] define an energy functional for image segmentation which takes into account the content of the interior and exterior regions of the curve (or surface), in contrast with the GAC, which define its energy functional, taking into account only the

pixels' intensity gradients along the curves.
The ACWE functional of a curve $\mathcal{C}$ is:

$$\begin{aligned} F(c_1, c_2, \mathcal{C}) \; &= \mu \cdot \text{length}(\mathcal{C}) \; + \; \nu \cdot \text{area}(\text{inside}(\mathcal{C})) \\ &+ \lambda_1 \int_{\text{inside}(\mathcal{C})} \|I(\mathbf{x}) - c_1\| d\mathbf{x} \\ &+ \lambda_2 \int_{\text{outside}(\mathcal{C})} \|I(\mathbf{x}) - c_2\| d\mathbf{x}, \end{aligned}$$

where the non-negative parameters μ, ν , λ_1 and λ_2 control the strength of each term, while c_1 and c_2 evaluate the mean intensity inside and outside the contour:

$$c_1 = \frac{\int_{\text{inside}(\mathcal{C})} I(\mathbf{x}) d\mathbf{x}}{\int_{\text{inside}(\mathcal{C})} d\mathbf{x}}, \quad c_2 = \frac{\int_{\text{outside}(\mathcal{C})} I(\mathbf{x}) d\mathbf{x}}{\int_{\text{outside}(\mathcal{C})} d\mathbf{x}}.$$

In this case, the level set formulation, that has to be solved through morphological operators, reads as

$$\frac{\partial u}{\partial t} \; = \; |\nabla u| \left(\mu \; \text{div} \left(\frac{\nabla u}{|\nabla u|} \right) \; - \; \nu \; - \; \lambda_1 (I - c_1)^2 \; + \; \lambda_2 (I - c_2)^2 \right). \tag{2.5}$$

We will see in the following sections how these two morphological snakes are used and their effect on the segmentation.

2.1.4. Refinement

Although the geometry of the aorta helped us to obtain a first guess of the lumen, we still have to check the segmentation and solve possible issues.
The two most frequent problems are the missing segmentation of the lumen's aorta (for example after the bifurcation of the iliac arteries) and the over-expansion of the segmentation to smaller arteries attached to the aorta. Both problems can be solved exploiting morphological snakes.
For this part the `morphological_chan_vese()`, implemented in the `scikit` library, has been choosen, since it is faster and more suitable if we only have to perform a smoothing and an expansion in region with high intensity pixel values.
The algorithm has to minimize the functional defined in (2.1.3), exploiting the level set formulation (2.5). We have already seen in the previous chapter that the key to solving the equation is evolving the contour through successive application of the morphological operators. In practice, we use the discretized version of them. The *dilation* D_h and

erosion E_h are approximated by

$$D_d(p(i,j)) = \max_{\delta i, \delta j \in \{-1,0,1\}} p(i+\delta i, j+\delta j)$$

$$E_d(p(i,j)) = \min_{\delta i, \delta j \in \{-1,0,1\}} p(i+\delta i, j+\delta j)$$

In other words, the new value of a contour's pixel p depends on the 8 neighborhood pixels and p itself. The complete description of the algorithm and the approximations of other morphological operators can be found in [5].
If we look at Figure (2.9) , we notice how the operator is able to improve the segmentation. We underline that the z-axis consistency it is crucial, because without it the operator could not be able to detect irregularities between different slices.

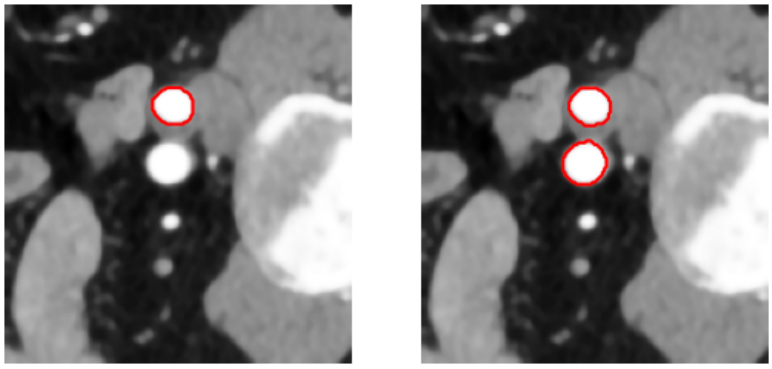

Figure 2.9: Segmentation before and after the morphological operators. (Patient 1)

At the end of the refinement, we obtain a smoothed guess of the lumen, consisting of the aorta and the iliac arteries. Even if the smoothed guess is enough to detect the thrombus and the calcifications, it could be useful detecting also the renal arteries. In fact, their detection could give the doctors important information to better understand where the aneurysm develops. We perform an additional refinement localized to the renal arteries, which are positioned right below the mesenteric vessel. We recall that we already know the position of the mesenteric artery since we use it to crop the initial VOI.

2.1.5. Other tissues

In every CTA scan, other tissues could be segmented apart from the three structures that we have to detect. Looking at Table (1.1) we notice that the spine (bones) has the highest HU attenuation value and hence could be easily detected, moreover, all the arteries in which the medium flows are displayed in bright colors.
The spotting of the spine and the arteries is mandatory for two main reasons. The first

reason is about completeness, instead of having just the lumen and the thrombus it is better to detect also all the structures, which could be helpful for the doctors. The second reason is purely practical, indeed the segmentation of the spine and other vessels is used in the thrombus detection.

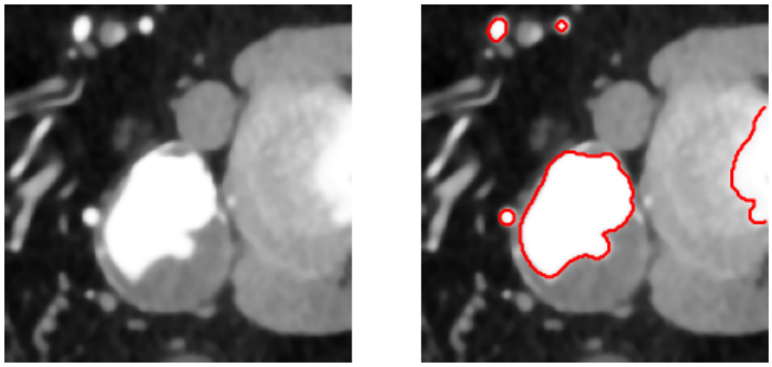

Figure 2.10: Segmentation of lumen, spine and arteries. (Patient 1)

The same process of refinement through morphological operators is applied for arteries and spine, but we have to re-scale the image with different values of the parameters. We want to highlight even more the low-intensity tissues, hence we set $L = 40$ and $W = 50$. We do not perform smoothing on the new set of re-scaled scans because we already have an initial guess, therefore we do not have to detect contours, moreover, if we avoid the smoothing, we ensure that the black pixels between the thrombus and spine will not become brighter. For ease of understanding, we still show the contours on the smoothed CTA.

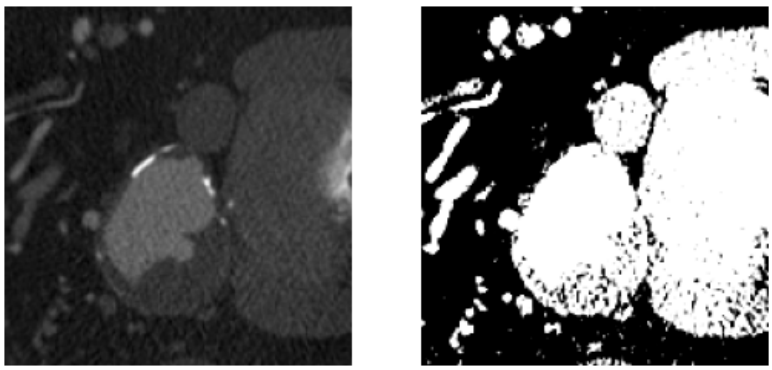

Figure 2.11: Effect of the re-scaling with $L = 40$ and $W = 50$. (Patient 1)

From Figure (2.12) we see how important is the refinement for the spine, in fact, some slices contain the bones and the cartilage that has a lower intensity. Thanks to the refinement in all the scans both bones and cartilage are detected.

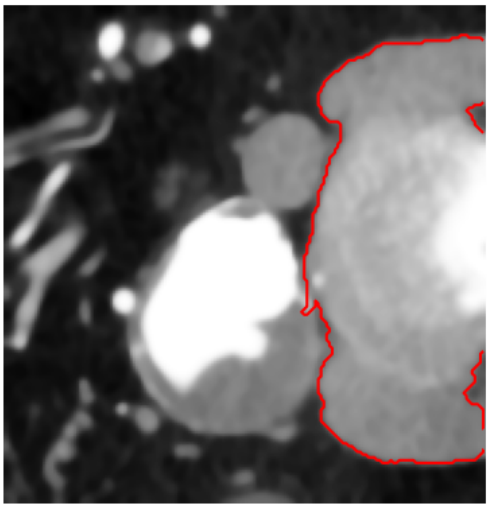

Figure 2.12: Segmentation of the spine and arteries. (Patient 1)

We also see that a little part of the spine segmentation extended inside the thrombus area. Anyway, if we consider the balance of benefits and risks, it is better to refine the spine as we did for mainly two reasons. The over-extension is only present in a few slices and, more importantly, it does not affect the thrombus segmentation too much if some precautions are taken in the next sections.

2.2. Thrombus segmentation

After the first part of the algorithm, we detected the lumen, the spine, and other vessels. The second and most challenging part is the segmentation of the thrombus.
As we have already seen in the previous pictures, the thrombus has an intensity that can be similar, sometimes equal, to surrounding tissues, therefore a more advanced segmentation strategy has to be implemented.

2.2.1. Image pre-processing

As we did for the lumen, we have to pre-process the CTA scans to facilitate the detection of the thrombus. The re-scaling is performed using (2.1), fixing $W = 200$ and $L = 40$. With this values the bounds are $\lambda^+ = 140\ HU$ and $\lambda^- = -60\ HU$. If we focus on λ^+ we notice that it decreased by 100 HU with respect to the bound used for the lumen, this allows us to display in brighter color even the thrombus, which has a lower Hounsfield attenuation value. The drawback of the re-scaling is that also the other tissues that are not thrombus are more visible and hence more likely to be segmented.

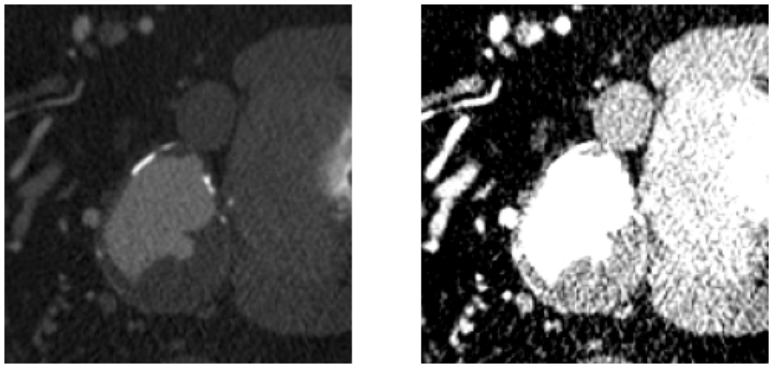

Figure 2.13: Effect of the re-scaling with $L = 40$ and $W = 200$. (Patient 1)

After the re-scaling, we smooth the image with the same `itk` filter but with different parameters. This time we lose some homogeneity but in exchange, we preserve some black pixels which are necessary to distinguish the aneurysm from the other structures.

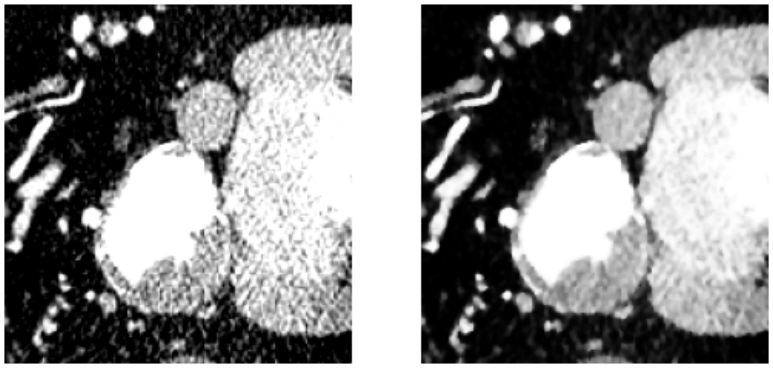

Figure 2.14: Segmentation before and after the smoothing. (Patient 1)

Now we can go further and exploit the previous steps. At the end of the lumen segmentation, we decided to detect the spine and vessels, which of course are not part of the aneurysm. Consequently, we can simply remove their segmentation from the pre-processed CTA scans.

This trick partially solves the problem of over-expansion in unwanted regions and gives us the starting point for the thrombus segmentation.

2.2.2. Segmentation

The segmentation of the thrombus represents the most challenging part due to the anatomy of the patients. The thrombus can have different shapes and dimensions, moreover, it can be easily confused with surrounding tissues having the same intensities.

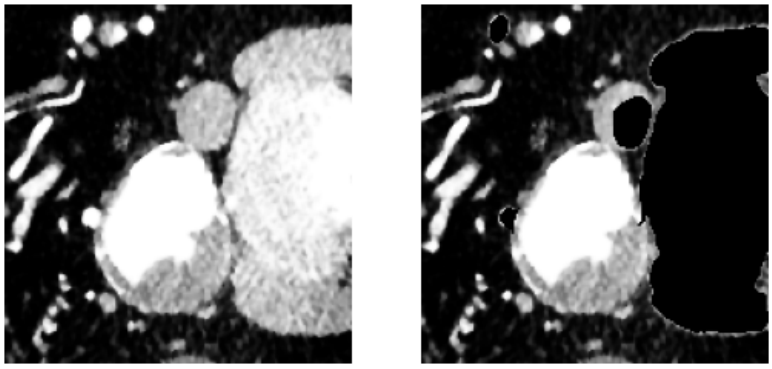

Figure 2.15: Effect of the deletion of spine and vessels. (Patient 1)

For those reasons, the segmentation cannot be done in just one step but it has to be divided into sub-problems. In particular, three main steps are performed to get the final segmentation:

- Over expansion,
- Reshaping,
- Refinement.

Now we will go through each of these steps, focusing on the implementation and the problems that they address.

Over expansion

The first stage has been developed to cope with the problem of the thrombus's low intensity. Even after the re-scaling, some parts of the thrombus could remain not well defined, and this could lead to an underestimation of the thrombus's dimension, which is the most important indicator to decide whether to operate or not.
To guarantee that the aneurysm is not under-estimated we can perform an enhancement of the intensity of the pixels. The latter constitutes a sort of hard re-scaling in which the value of some pixels is increased to a higher value. Practically speaking, we need to enhance the value of the pixels corresponding to the thrombus, but, since we do not have this information, we set a range of intensity P and we change all the pixels within that range. For example

$$P = [90, 140], \quad p = \begin{cases} 180 & if \quad p \in P, \\ p & otherwise. \end{cases}$$

The choices of the range and the new intensity are not patient-dependent but they have been tuned during the development looking at different CTAs.

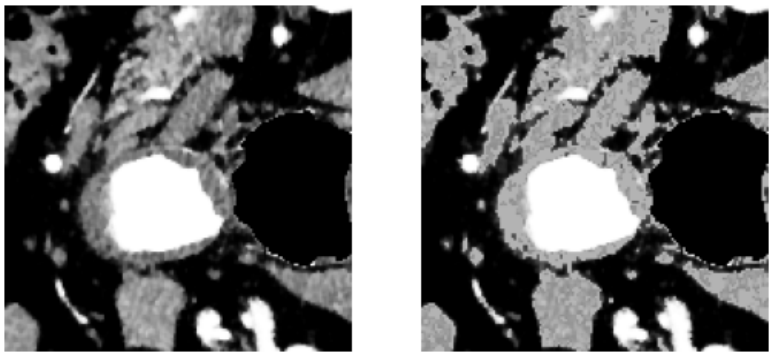

Figure 2.16: CTA before and after the pixel enhancement. (Patient 2)

From Figure (2.16) we can note that the operation enhances the pixels of the aneurysm correctly, but also brightens the pixels of blood vessels near the thrombus. This problem is addressed in the next steps, now we have to make sure that all the thrombus is detected. The detection of the thrombus becomes straightforward now that we have the enhanced CTA. Exploiting the lumen's guess and the operator `morphological_chan_vese()`, we can expand the initial segmentation towards the thrombus.

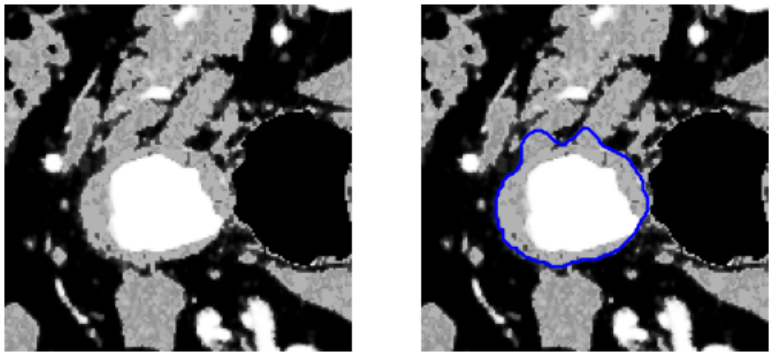

Figure 2.17: Over expansion of the morphological snake. (Patient 2)

Figure (2.17) confirms what we said above. The morphological snake detects the thrombus, it expands through other blood vessels and it stops when the number of iterations is reached.
Intuitively we should try to find the right number of iterations so that the thrombus is detected while the other tissues are neglected, but is clear that this approach is not robust and is patient-dependent. We let the morphological snake expands and then in the next steps we modify the contour exploiting the shape of the thrombus.

Reshaping

After the application of the morphological snake on the enhanced CTA, we have a first guess of the aneurysm but with some ill-detected extensions, mainly blood vessels close the thrombus. The reshaping technique addresses the problem, exploiting the shape of the aneurysm, which could have different dimensions but usually, it develops in a circular/oval form. A way to remove the spurious extensions of the segmentation could be performing an image convolution.
An image convolution is an operation that consists in going through each image's pixel p, and performing a calculation between p and its neighbors pixels. This process needs:

- input image,
- morphological operator,
- convolution matrix.

The input image could be a segmentation in a fixed slice, id est a 2D matrix filled with 0 (pixel detected as not thrombus) and 1 (pixel detected as thrombus). Then we need to choose the morphological operator, which could be *erosion*, *dilation* or a combination of them. The last ingredient is the convolution matrix, or kernel, which decides how the pixels interact with each other. In particular, the kernel is a 2D matrix that indicates, for the currently processed pixel p, which are the neighbors to consider during the computation. The kernel's element could be 1 (neighbor to consider), or 0 (neighbor to not consider). Moreover, the matrix could be 3×3, including only the adjacent neighbors of p, or could have larger dimensions, if we want to take into account more distant pixels. Together with the kernel, we also select the anchor point, which defines how the kernel is positioned with respect to the pixel p currently processed during the operation.
To better understand how it works, let's say we want to perform an *erosion* on a 2D image. We select a kernel defined as:

$$K = \begin{pmatrix} 1 & 1 & 1 \\ 1 & 1 & 1 \\ 1 & 1 & 1 \end{pmatrix},$$

with anchor point at the center of the matrix.
We already saw the definition of *erosion* and *dilation*, here we give an equivalent interpretation. The *erosion* is a morphological operator that given a pixel p and a set B with N_B pixels, sets $p = 1$ if all the pixels in B are equal to 1, otherwise it sets $p = 0$. In other

words:

$$E(p, B) \;=\; 1 \iff b_i = 1 \quad \forall\, i = 1, \ldots, N_B$$

This operation is performed on every pixel p of the original image and for each pixel the set B is obtained trough the kernel K. In our case, since the anchor point is at the center of the matrix, the set B contains the current pixel p and the 8 neighborhood pixels. If instead K was defined as:

$$K = \begin{pmatrix} 0 & 0 & 0 \\ 0 & 1 & 0 \\ 0 & 1 & 0 \end{pmatrix},$$

with anchor point at the center of the matrix, the set B would have contained only the current pixel p and its underlying neighborhood. So that changing the values and the dimension of K changes the effect of the *erosion*, the larger and fuller the matrix, the stronger the *erosion*.
The dilation follows the same idea, but with a different definition:

$$D(p, B) \;=\; 1 \iff \exists\, b_i = 1 \quad i = 1, \ldots, N_B$$

For our purpose the first thing to consider is that the dimension of the thrombus along the z-axis can change, hence we have to iterate through the segmentation's slices and perform the reshaping of our guess on the 2D segmentation and not on the whole volume. For each slice we select the segmentation's contour and we evaluate its length, this give us information about the dimension of the thrombus in that slice.
At this point we want to perform a 2D convolution using a combination of *erosion* and *dilation* called *opening*. In particular we apply the *erosion* operator first, to remove the spurious extension, then we exploit the *dilation* to recover the size of the original segmentation. The last crucial step is the choice of the kernel. Since we observed that the aneurysm has a circular shape we can select an elliptical kernel, which has the form:

$$K = \begin{pmatrix} 0 & 0 & 0 & 1 & 0 & 0 & 0 \\ 0 & 1 & 1 & 1 & 1 & 1 & 0 \\ 1 & 1 & 1 & 1 & 1 & 1 & 1 \\ 1 & 1 & 1 & 1 & 1 & 1 & 1 \\ 1 & 1 & 1 & 1 & 1 & 1 & 1 \\ 0 & 1 & 1 & 1 & 1 & 1 & 0 \\ 0 & 0 & 0 & 1 & 0 & 0 & 0 \end{pmatrix}.$$

The kernel shown above is an example of elliptical kernel with dimension 7. In the

algorithm, the dimension is evaluated computing the radius from the length of the segmentation's contour. In other words:

$$K \in \mathbb{R}^{r\times r},\ r\ = \left\lfloor \frac{length(\text{contour})}{2\pi} \right\rfloor.$$

The functions used for the reshaping are taken from the `OpenCv` library which implements morphological operations with different kernels. Now that we have all the ingredients we can iterate trough the slices and perform the reshaping.

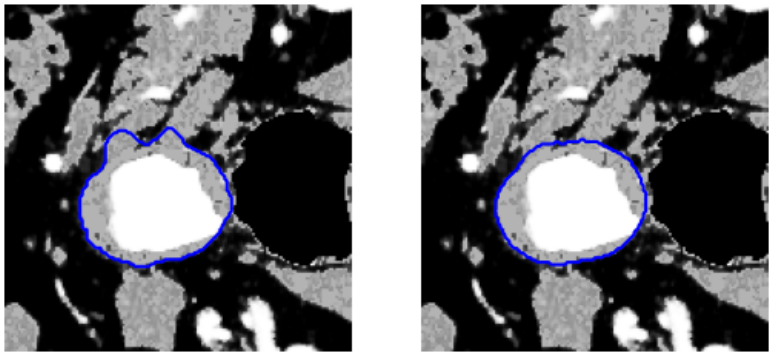

Figure 2.18: Segmentation before and after the reshaping. (Patient 2)

From Figure (2.18) we see the effect of the convolution on the contour, in particular we can observe that the spurious extensions are removed and the contour has a smoother behaviour.

The reshaping gives us a double advantage. First of all, as we have seen, it transforms our first segmentation into a more realistic guess of the thrombus, second of all, it identifies the spurious extensions. We can remove them as we have done for the spine, by computing the difference between the two segmentations and subtracting it from the original slice. In this way, we give as input for the next steps a CTA in which for sure the segmentation cannot grow towards tissues that are not part of the thrombus.

As we can see from Figure (2.19) now in the CTA black pixels substitute the spurious extensions, preventing the segmentation to grow towards that region.

Refinement

In some patients, after the reshaping part, we have already a good segmentation of the aneurysm, but a refinement process is still mandatory. We recall that the reshaping has

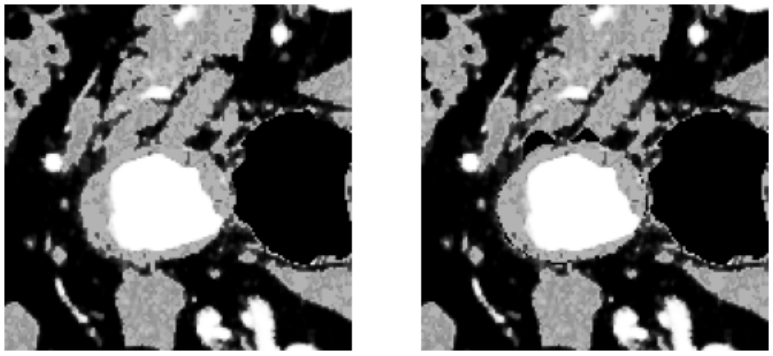

Figure 2.19: CTA before and after the removal of the spurious extensions. (Patient 2)

been performed on the single slice, hence not taking into account an axial consistency along z, moreover, we need to adjust the segmentation where the previous step has partially failed.
This last refinement step is carried out by a different morphological snake, the `morphological_geodesic_active_contour()`. The definition and the difference with the other operator have already been discussed in (2.1.3), here we focus on the actual features of the morphological snake.
The morphological GAC has the advantage of being more conservative, it does not simply expand in regions with similar pixels' intensity, but it tries to stop when an edge of the object is encountered. Therefore, we need to highlight the borders of the thrombus in the CTA scans. We can perform this transformation using the function `inverse_gaussian_gradient()` of the `scikit` library. Given an image as input, it computes the magnitude of the gradients in the image, hence for flat areas where the pixels have the same intensity the gradient will be 0 or very small. Near the edges, where there is a fast transition and therefore a sharp difference between the pixels, the gradients will be very high. In practice, the output image will have inverted values, flat areas are assigned values close to 1, while areas close to borders are assigned values close to 0.

In Figure (2.20) we can distinguish two main edges, the first one is between the lumen and the thrombus, and the second one is between the thrombus and the exterior. Since our guess starts outside of the lumen, it stops on the second edge, which is the one that we are interested in. Notice that if we have started the thrombus segmentation directly from this step we would have encountered difficulties since our first guess was the lumen segmentation and the algorithm would have not been able to expand through the first edge. We can also observe that the removal of the spurious extensions has the effect of creating a sharp gradient between the thrombus and other tissues, which suits perfectly

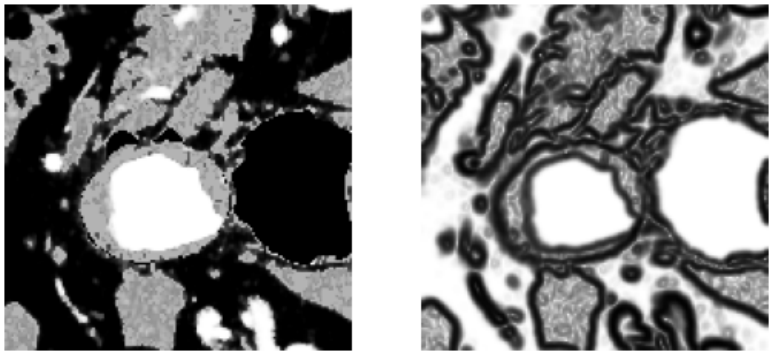

Figure 2.20: CTA and CTA's magnitude gradients. (Patient 2)

for our intent.
Figures (2.21) and (2.22) show the effect of the refinement. In the first case, only minor changes are made to the segmentation, in the second we see the importance of the morphological GAC.

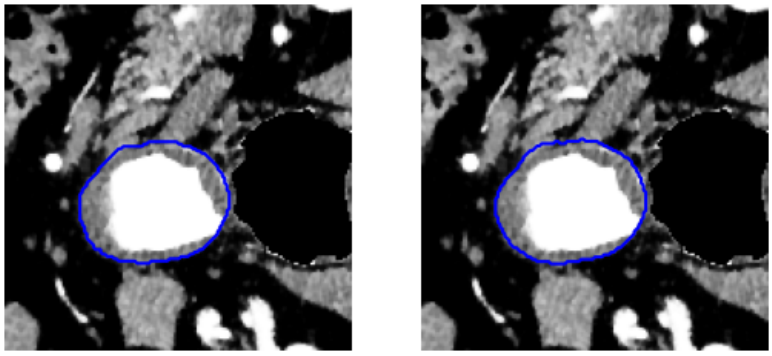

Figure 2.21: Segmentation before and after the morphological GAC. (Patient 2)

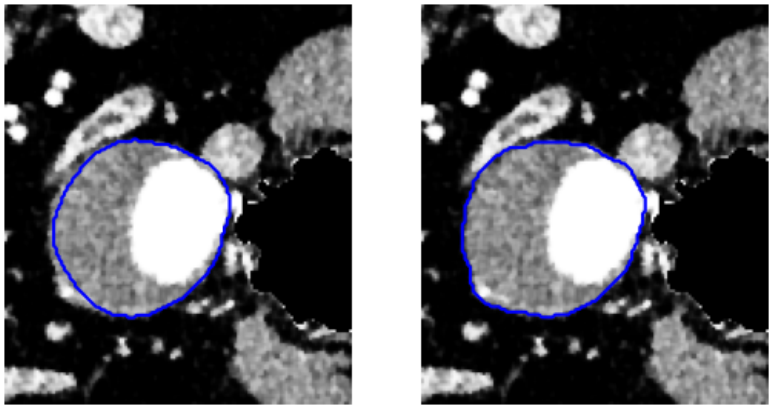

Figure 2.22: Segmentation before and after the morphological GAC. (Patient 3)

Before leaving the thrombus segmentation we perform a localized last refinement. Right above the iliac bifurcation the thrombus changes dimension rapidly and could have irregular shapes. Due to this behavior, the reshaping part could fail and could give poor input to the refinement part, such as CTA scans in which the thrombus has been removed because considered as other tissue. To solve this problem, we perform an additional refinement localized to the iliac bifurcation. The procedure is the same as before, but the input of the morphological snake changes. In the former refinement, we removed the spurious extension from the CTA scans before using the morphological GAC. This time, we omit the removing part so that we can segment the part of the thrombus that had been wrongly removed.

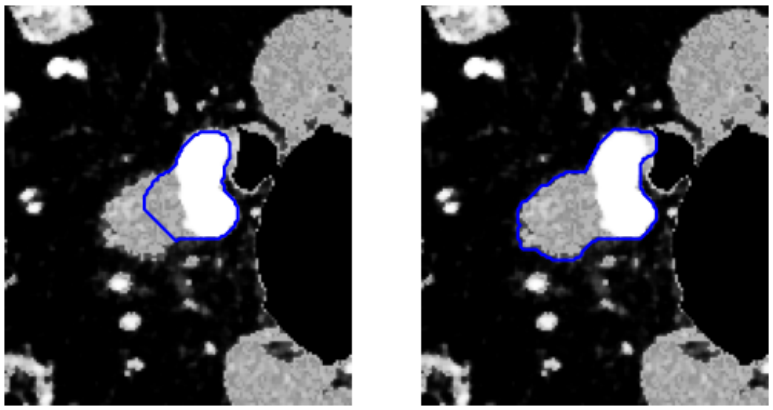

Figure 2.23: Segmentation before and after the localized refinement through GAC. (Patient 3)

2.3. Calcifications

Calcifications are accumulations of calcium which are located on the walls of the aorta. We recall that calcium has a high Hounsfield value, therefore the challenge is not identifying the calcifications but choosing where to search them. This fact makes the segmentation of the calcifications strongly dependent on the detection of the lumen and the thrombus.

2.3.1. Image pre-processing

Calcifications divide into two types. The first ones are located on the walls of the healthy aorta, where there are no blood clot, and their characteristic is the strong brightness even in the raw CTA (not re-scaled).
The second type, which is placed on the thrombus's walls, usually has a lower intensity, therefore its segmentation needs a re-scaling of the input image. In particular, we will use

(2.1) with $W = 400$ and $L = 40$, the same parameters used for the lumen.

2.3.2. Segmentation

We start by detecting the calcifications with high brightness. We loop over the CTAs and for each slice, we select the domain in which we will search the calcification. The region of interest is obtained by exploiting the segmentation of the lumen. Since we know that the calcium builds up on the artery's wall, we can dilate the original lumen segmentation to obtain a slightly bigger region, then we erode the original segmentation to get a smaller one. Finally, we take the difference of these sub-regions, which has a ring-shape, and we apply it, as a mask, to the CTA.
Since the lumen's guess should contain the calcifications, we usually need a small kernel for the *dilation*, while it is better to use a big kernel to get a stronger *erosion*. In the code we selected $K_{erosion} \in \mathbb{R}^{12\times12}$ and $K_{dilation} \in \mathbb{R}^{2\times2}$, both the matrix filled with ones.

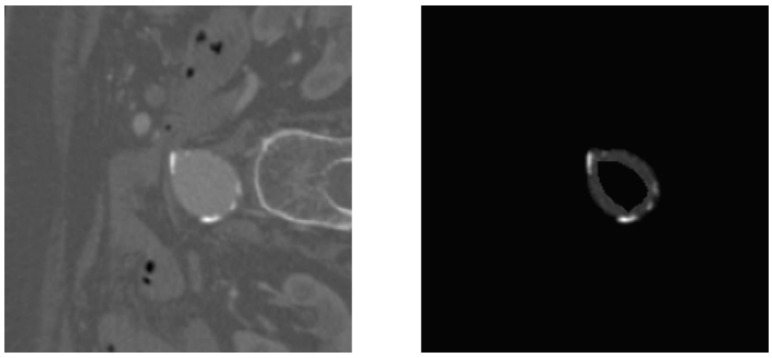

Figure 2.24: Ring-shaped mask for the lumen calcifications. (Patient 4)

Then we apply a threshold on the ring-shaped region to detect the calcifications.

Figure 2.25: Threshold for the lumen calcifications. (Patient 4)

The same procedure applies to the segmentation surrounding the thrombus. The main

differences are that we use the thrombus segmentation instead of the lumen's and we use a re-scaled CTA to enhance the calcifications.

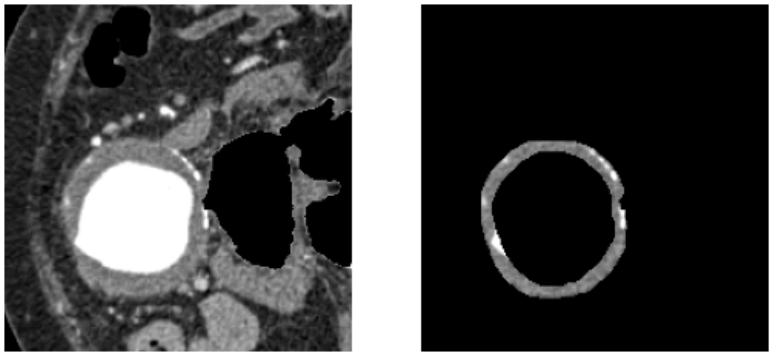

Figure 2.26: Ring-shaped mask for the thrombus calcifications. (Patient 4)

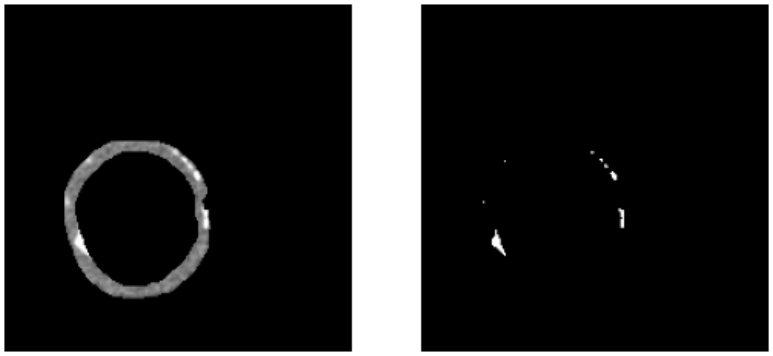

Figure 2.27: Threshold for the thrombus calcifications. (Patient 4)

As we can see from Figure (2.27) if we use a re-scaled CTA also the lumen is enhanced and could be detected as calcification. This problem is trivially solved by removal the lumen's segmentation from the threshold.
At the end of the detection we exploit once again the morphological operators *erosion* and *dilation* to remove isolated pixels which are wrongly selected by the threshold.

2.4. Indicators

We started the discussion by saying that the detection of the aneurysm could help doctors and support them in the pre-surgery decisions. The 3D segmentation gives us an overview of the thrombus' shape and dimension, but it does not give quantitative information. In the literature [19], many indicators that could be useful, have been defined. Our goal for this last section is to implement the most meaningful quantitative indicators and evaluate them for each patient.

Figure 2.28: Removal of the lumen. (Patient 4)

The first indicators which can be computed are the volumes, V_i, of lumen, thrombus, and calcifications. However, instead of looking at the absolute quantities, it is more useful to provide the relative volumes, RV_i, expressed as percentage of the whole volume, formed by the union of the three segmentations. The percentages give us a first quantitative sight of the dimension of the aneurysm and the presence of calcifications. The definitions are straightforward:

$$V_i = (\#pixel_i) \cdot (spacing)^3, \quad RV_i = \frac{V_i}{V_{tot}} \cdot 100,$$

where i can be referred to calcifications, lumen or thrombus, while $\#pixel$ is the number of pixels composing the segmentation and *spacing* is the physical dimension of a pixel's edge.

The next step to define other indicators is the computation of the vessels' centerline. A precise definition of centerline can be given as the line drawn from the two outermost sections of a tubular structure which locally maximizes the distance from the vessel boundary (see [20] to have more information). In order to compute the centerlines we exploit the `vtk` and `vmtk` libraries. In particular, we will use `vtk` to extract the surface of our segmentations, while we will take advantage of `vmtk` to actually compute the centerlines [20]. This process is performed both on the healthy lumen and the lumen plus the aneurysm, such that we can quantify the effects of the pathology with different indicators.

As already said in Chapter 1, current medical guidelines suggest that the surgery is the only way to go when the aneurysm grows excessively. Therefore, the maximum diameter, D_{max} of the aneurysm is for sure an indicator that has to be computed. To evaluate the maximum diameter, we iterate through the points $\mathbf{p}$ of the centerline, where we evaluate the local normal vector $\mathbf{n}$ as the unitary vector tangent to the centerline at the point. Then we construct a plane π passing trough $\mathbf{p}$ with normal $\mathbf{n}$, and we intersect it with the segmentation. This gives us the slice of the segmentation perpendicular to the centerline in a given point, from the latter slice we evaluate the diameter. We underline that the

maximum diameter is computed as that of the smallest circle enclosing the intersection.

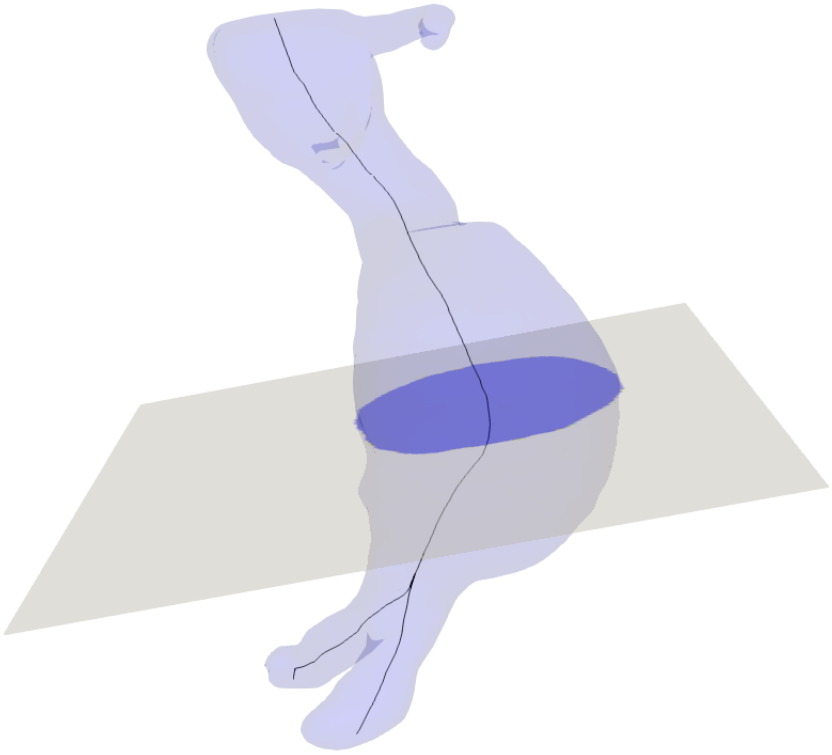

Figure 2.29: View of a vessel's section (Patient 4)

The last indicators that we compute are the tortuosity τ and the asymmetry factor β. The tortuosity can be defined as:

$$\tau = \frac{length(\text{centerline})}{straight\_length} - 1,$$

where $straight\_length$ is the Euclidean distance between the ends of the centerline. A value of τ close to 1 indicates a straight vessel while a small value of τ is symptom of a curved artery.
The asymmetry factor [19] is a measure of how distant the lumen's and thrombus' centerlines are, more precisely:

$$\beta = 1 - \frac{d_c}{D_{max}},$$

where d_c is the distance between the lumen centroid and the thrombus centroid of the cross section where the maximum diameter, D_{max}, is located. If $\beta = 1$ the two centerlines coincides on the slice containing the bigger section of the aneurysm, hence the lumen is

located more or less at the center of the thrombus, if instead β is close to zero, it is likely the the aneurysm has not developed homogeneously around the aorta.

3 | Numerical results

Now we show and comment on the results of the algorithm, which has been tested on four different patients with abdominal aortic aneurysm. Unfortunately, we could not get the segmentations provided by an expert, therefore we could not measure the errors between the automatic and the manual segmentation. However, we could still judge the work of the algorithm by looking at the CTA scans combined with the segmentation.

3.1. Lumen

We started the work detecting the lumen, which, we recall, is the passageway through which the aorta's blood flows. The algorithm based on the shape and the intensity of the aorta works fine, it is able to detect the aorta without meaningful errors. Another positive result is the robustness of the algorithm which, even without changing parameters, provides good detection for each patient.
From the lumen segmentation we can immediately notice how the iliac arteries are attached to the aorta and, more importantly, we can spot the region, right above the iliac bifurcation, on which the aneurysm will grow. Moreover, we visualize how the renal arteries develop. Concerning this last point, in Patient 4 there are two exceptions. First of all the VOI contains the mesenteric vessel, which is correctly detected, but, unfortunately, the renal arteries are not well displayed from the CTA scans, hence we identify only the beginning of their attachment to the aorta.
The last thing that we can observe from the lumen segmentation is the variety of anatomy that the aorta can have. The latter is one of the main problems which make the aneurysm's detection not trivial.

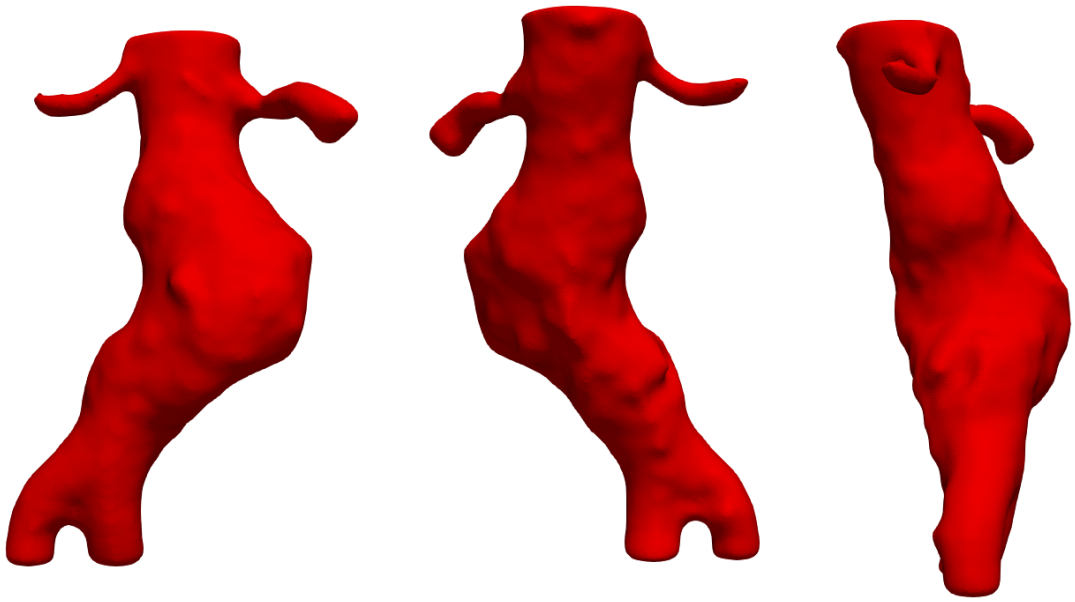

(a) Frontal view (b) Posterior view (c) Lateral view

Figure 3.1: Lumen segmentation of Patient 1

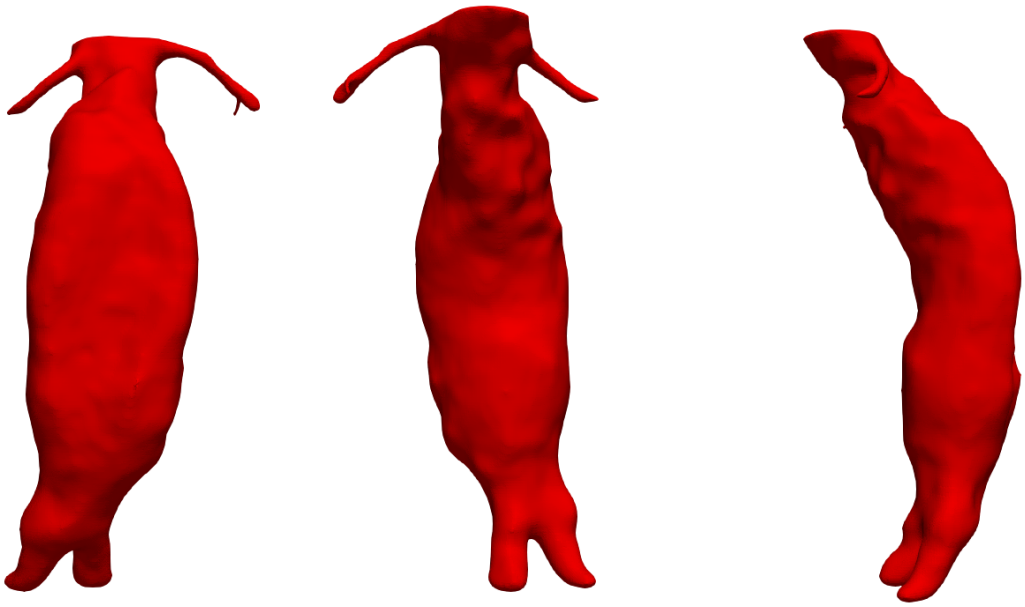

(a) Frontal view (b) Posterior view (c) Lateral view

Figure 3.2: Lumen segmentation of Patient 2

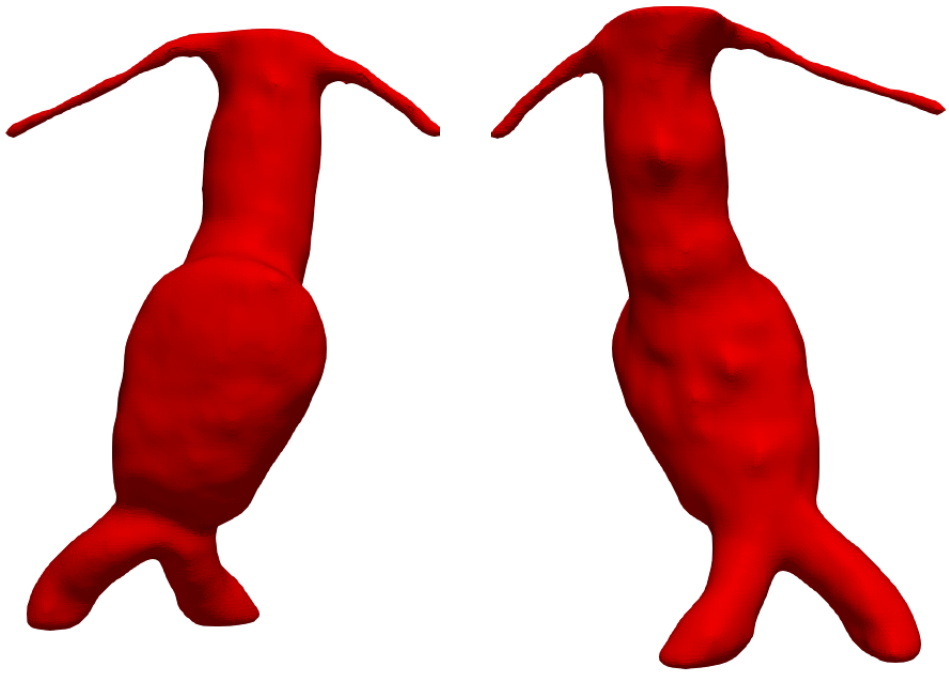

(a) Frontal view

(b) Posterior view

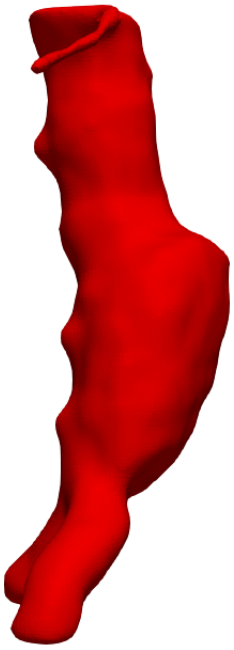

(c) Lateral view

Figure 3.3: Lumen segmentation of Patient 3

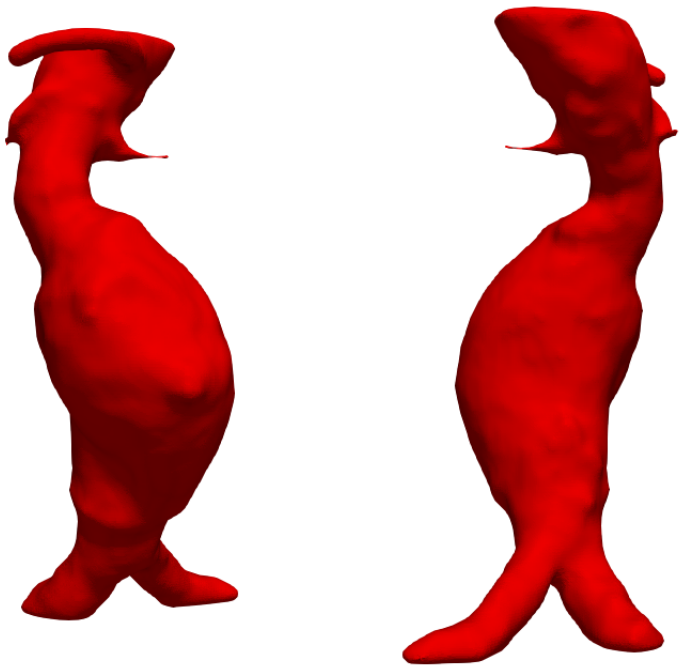

(a) Frontal view

(b) Posterior view

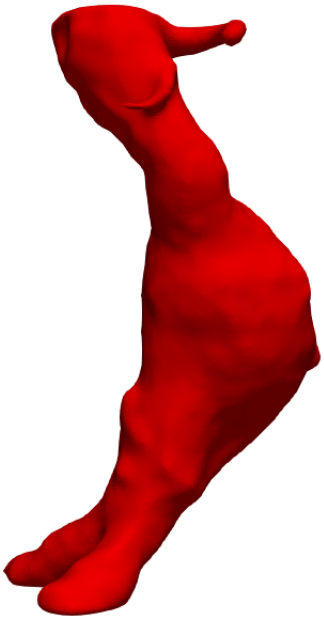

(c) Lateral view

Figure 3.4: Lumen segmentation of Patient 4

3.2. Thrombus

The main goal of the automatic tool was the detection of the aneurysm, from which we can extract useful quantities for the doctor. In Figure (3.5) - (3.6) - (3.7) - (3.8) the thrombus segmentation is shown. The surface of the aneurysm is displayed with a decreased opacity to enable seeing the difference with the lumen segmentation.
Since the detection of the thrombus was the most challenging part, it is worth showing some particular slices to see the effectiveness of the algorithm. Figure (3.9) shows two slices of Patient 1, in particular in the first we see how the algorithm is able to detect shapes that are not purely oval, while in the second we notice that even if another artery is attached to the thrombus the algorithm is capable to stop the expansion towards the vessel. In Figure (3.10), instead, we understand the importance of a morphological snake (GAC) that evaluates the gradient of an image. In fact, relying only on the intensity would have expanded the segmentation even further the aneurysm, since there is a high intensity region surrounding the thrombus.

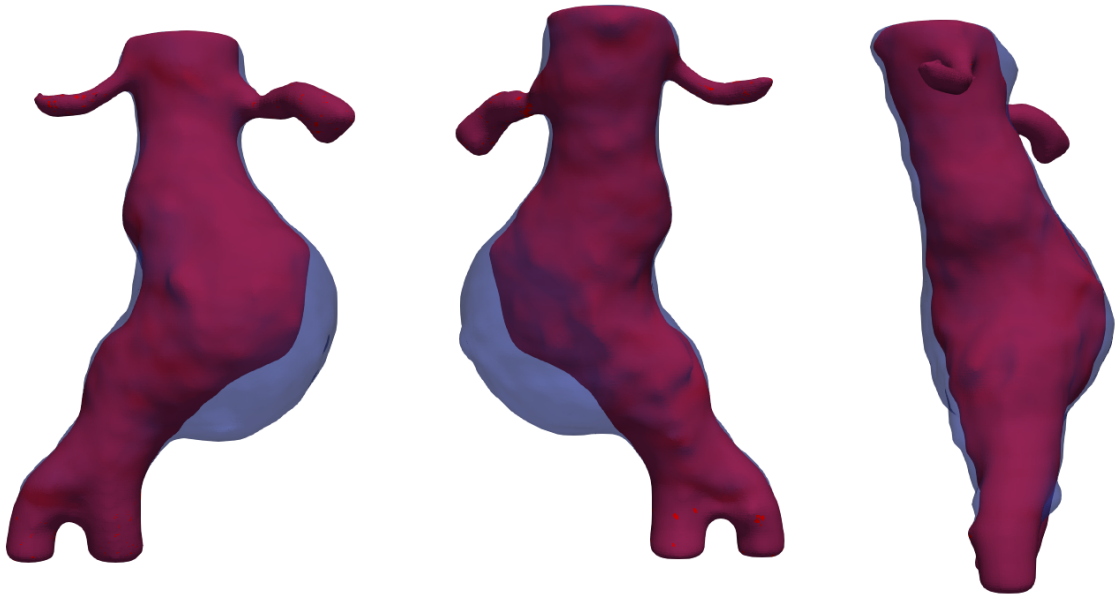

(a) Frontal view (b) Posterior view (c) Lateral view

Figure 3.5: Thrombus segmentation of Patient 1

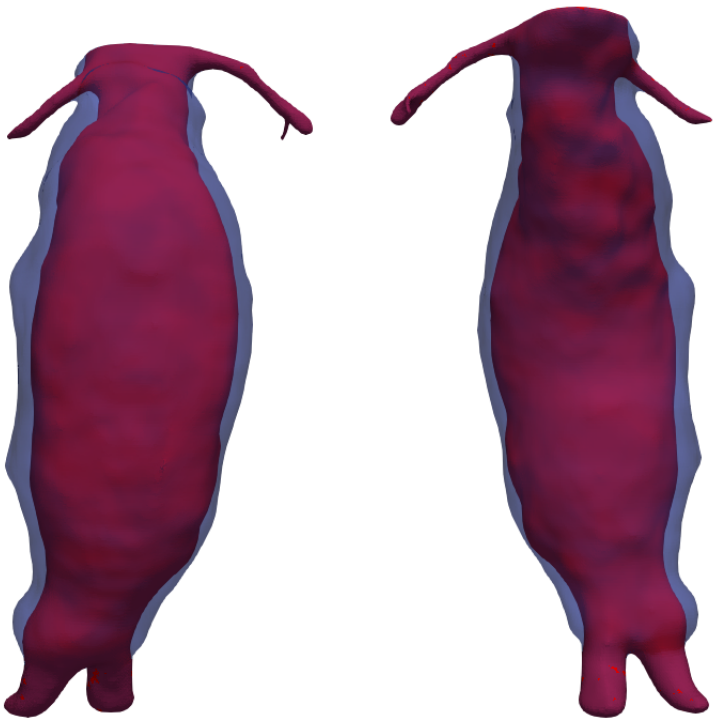

(a) Frontal view

(b) Posterior view

(c) Lateral view

Figure 3.6: Thrombus segmentation of Patient 2

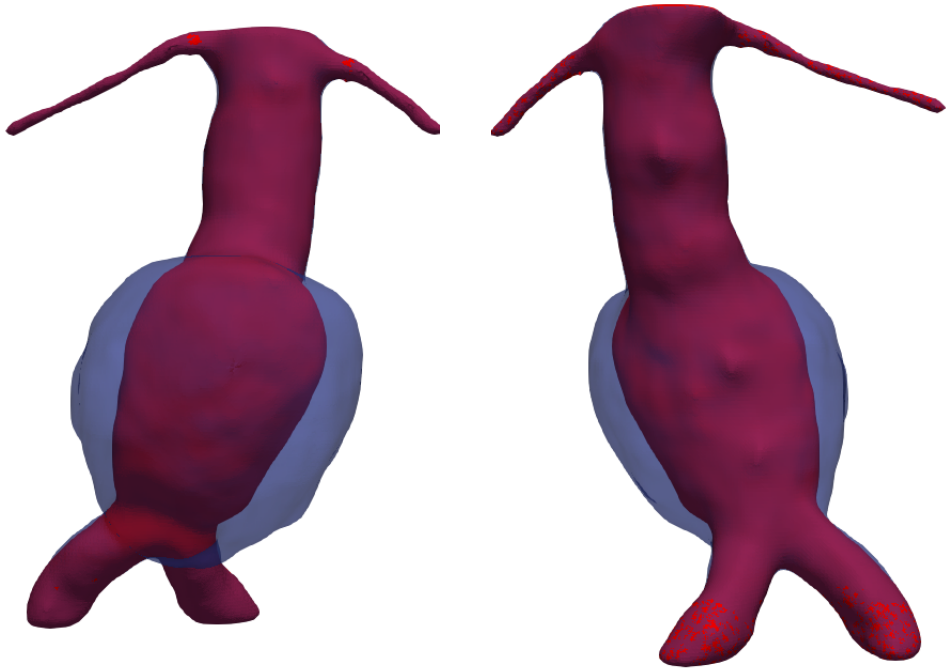

(a) Frontal view

(b) Posterior view

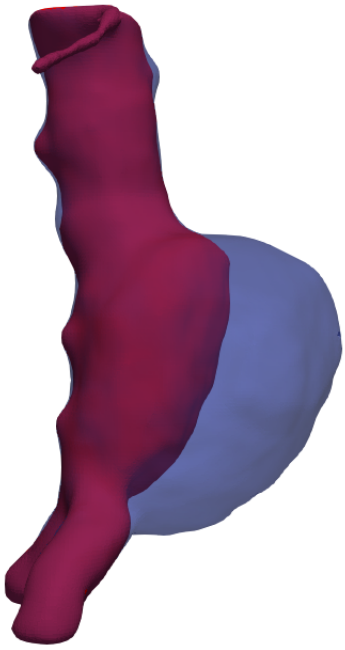

(c) Lateral view

Figure 3.7: Thrombus segmentation of Patient 3

(a) Frontal view

(b) Posterior view

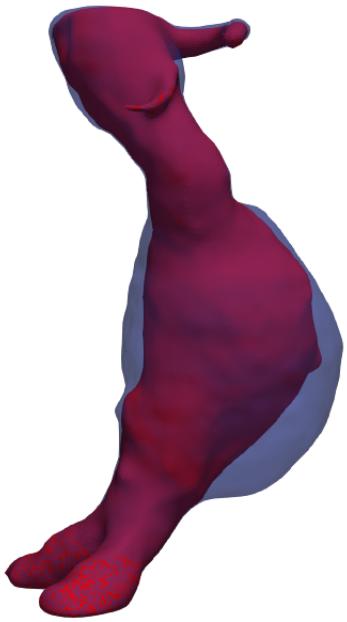

(c) Lateral view

Figure 3.8: Thrombus segmentation of Patient 4

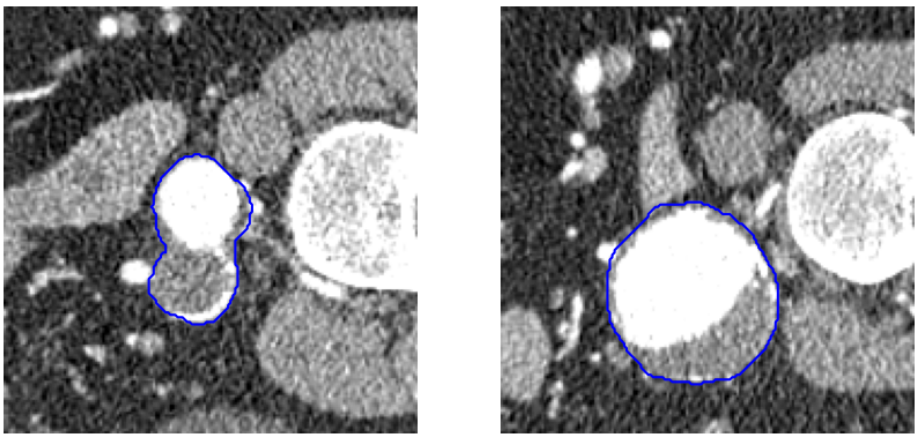

Figure 3.9: Slices of thrombus segmentation. (Patient 1)

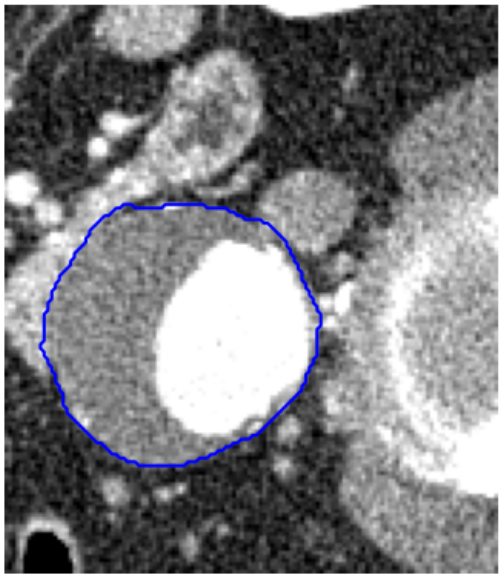

Figure 3.10: Slices of thrombus segmentation. (Patient 3)

The algorithm, in general, produces a precise detection of the aneurysm, however, errors are still present in some slices.

There are mainly two sources of errors. The first cause of errors is the reshaping part (2.2.2), which eventually could fail if the aneurysm has lots of irregularities. We already see in Figure (3.9) that the algorithm is able to detect irregular shapes, mostly due to refinement. However as we can see in Figure (3.11a) the algorithm partially detects the aneurysm, missing the outer part, while in (3.11b) it does not expand since it has detected the thrombus as spurious extension. We point out that this behavior often happens right above the bifurcation of the iliac arteries, where the dimensions of the aneurysm change

rapidly, and it is usually solved thanks to the last step of the refinement part (2.2.2).

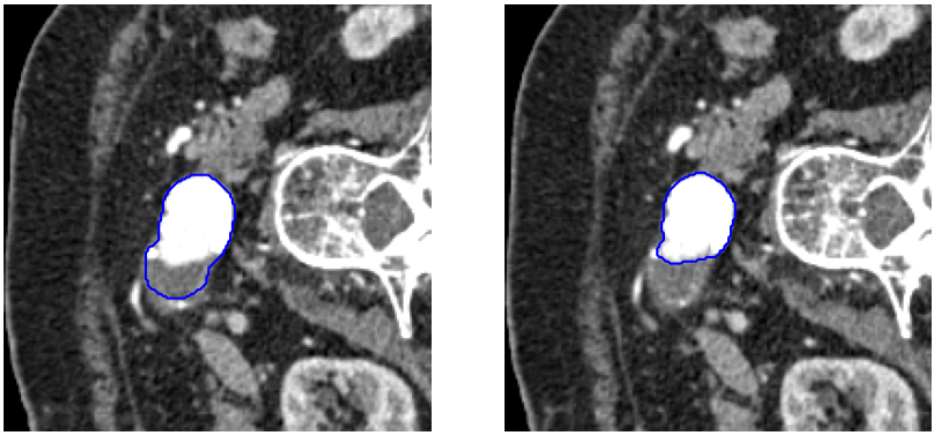

(a) Slice 144 (b) Slice 145

Figure 3.11: Errors in thrombus segmentation. (Patient 4)

The second type of error is the over-expansion which is more common and, unfortunately, more challenging to solve. The reshaping part gives us a way to block the segmentation towards other tissues, however, the anatomy of the patients could lead to wrong ovalizations. We can look at Figure (3.12) to see that if a tissue, with the same intensity of the thrombus, shares a boundary with the aneurysm could induce the detection to expand towards that tissue. Eventually, the reshaping will stop the expansion but the segmentation will contain a spurious detection. We can check this behavior also from Figure (3.6a) - (3.6b).

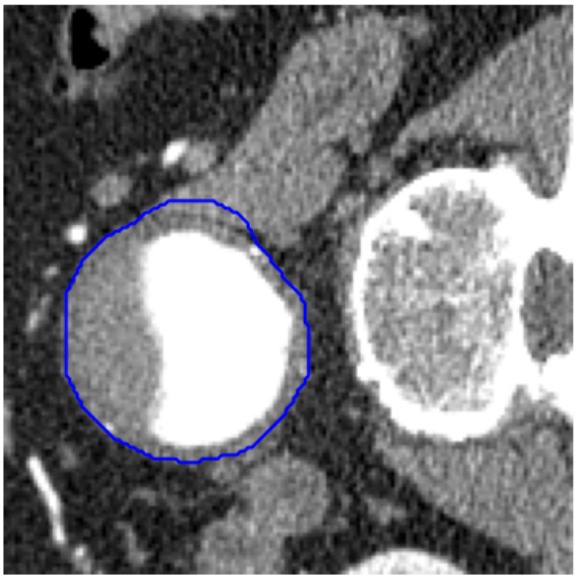

Figure 3.12: Error in thrombus segmentation. (Patient 2)

3.3. Calcifications

The third part of the algorithm consists in detecting the calcifications of the patients. As we can see from Figures (3.14) - (3.15) - (3.16) - (3.17), the quantity and the placing could vary from patient to patient, in particular in Patient 2 it seems that the presence of calcifications is almost nothing.
Looking at Figure (3.13) we can understand the importance of using a soft *dilation* while constructing the ring-shaped region. Indeed we can spot, right outside the thrombus, a little artery and the spine, which could be wrongly segmented if a stronger *dilation* was used.
Some errors could occur also in the detection of the calcifications. The great majority of them are caused by arteries and bones close to the aneurysm. In fact, even if we use a soft *dilation*, the ring-shaped region could contain other tissues with high intensity which will be segmented by the algorithm. An example is shown in Figure (3.18).

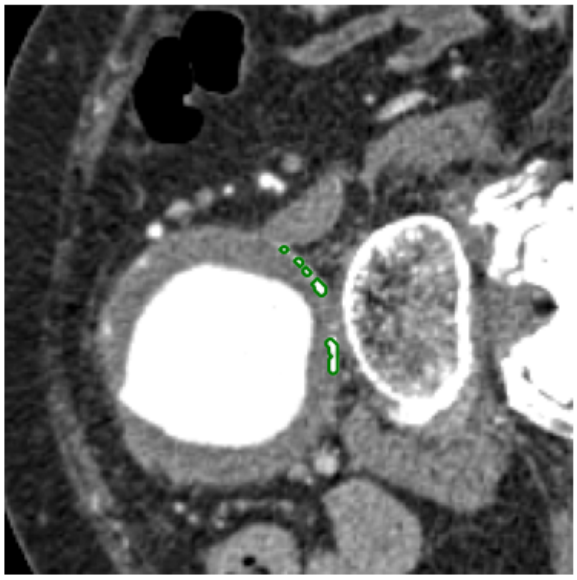

Figure 3.13: Calcifications segmentation. (Patient 4)

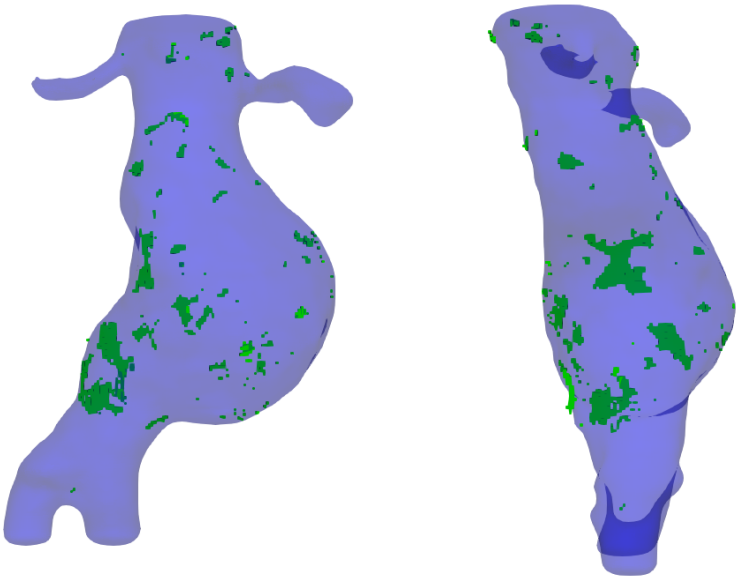

(a) Frontal view (b) Lateral view

Figure 3.14: Calcifications segmentation of Patient 1

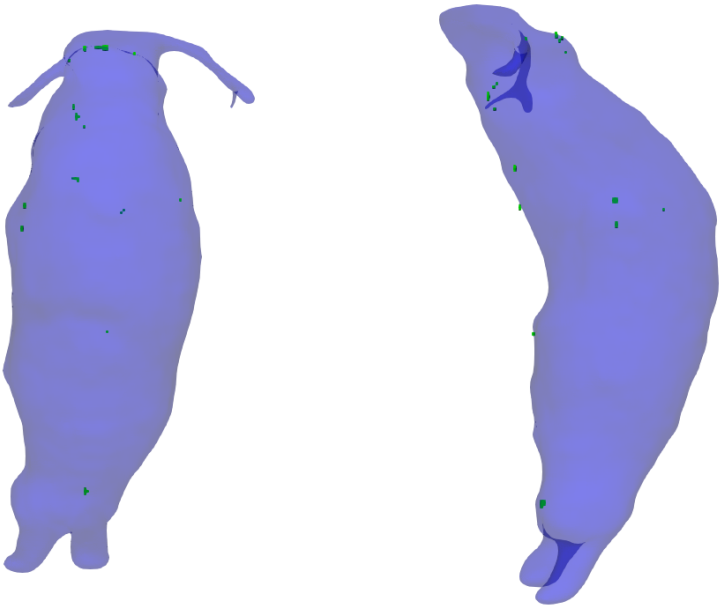

(a) Frontal view (b) Lateral view

Figure 3.15: Calcifications segmentation of Patient 2

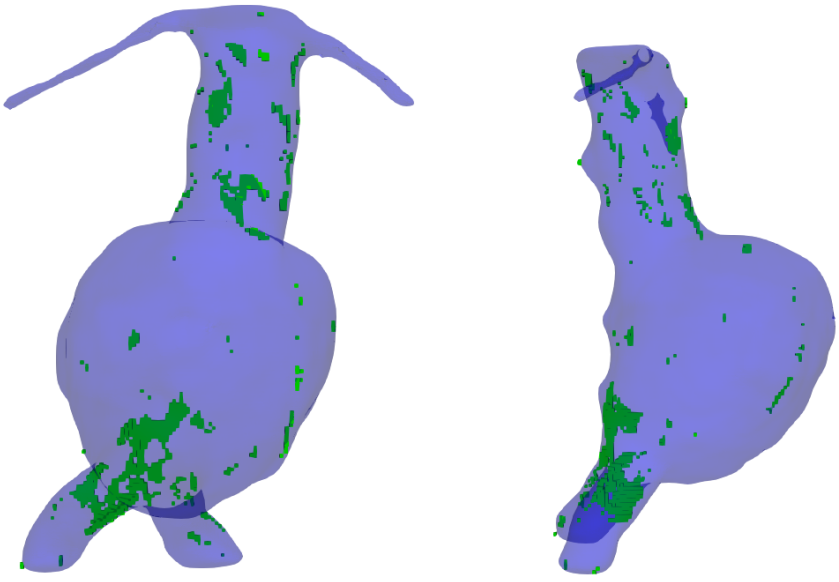

(a) Frontal view (b) Lateral view

Figure 3.16: Calcifications segmentation of Patient 3

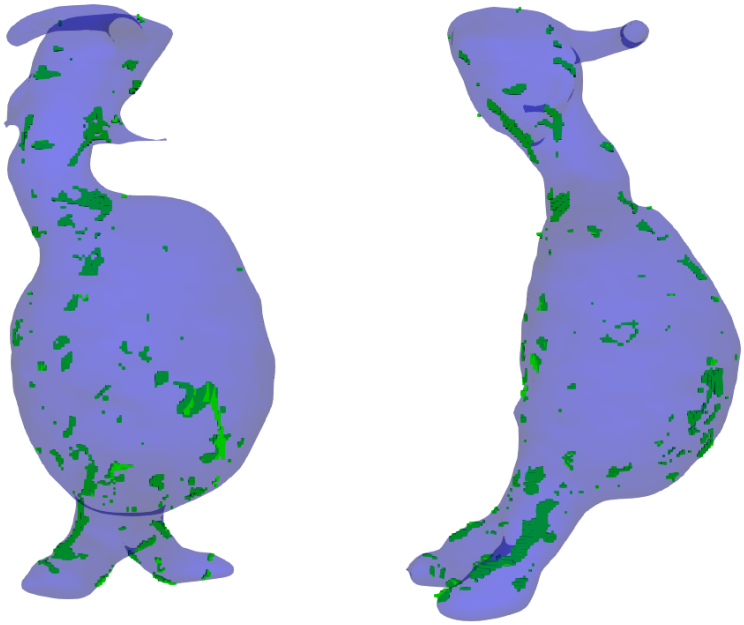

(a) Frontal view (b) Lateral view

Figure 3.17: Calcifications segmentation of Patient 4

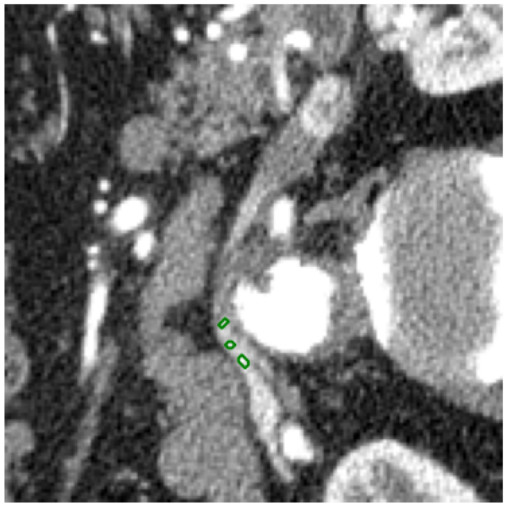

Figure 3.18: Error calcification detection. (Patient 2)

3.4. Indicators

In this last section, we comment on the indicators we have computed from the segmentations.

AAA indicators

	Patient 1	Patient 2	Patient 3	Patient 4
RV_{calcif}	2.04 %	0.2 %	2.05 %	1.66%
$RV_{thrombus}$	28.5 %	40.37 %	47.8 %	36.8%
D_{max}	51.1 mm	57 mm	60.3 mm	63.7 mm
$\tau_{thrombus}$	0.12	0.12	0.16	0.24
β	0.87	0.85	0.82	0.98

Table 3.1: AAA indicators for the four patients.

The first thing we notice from Table (3.1), is that three patients have a maximum diameter greater than 55 mm, which is the threshold to decide if surgery is needed. In particular, Patient 4 has a maximum diameter that exceeds the threshold by almost 1 cm, an event that increases dangerously the risk of rupture.
Another important indicator, to quantify the development of the aneurysm, is the relative volume. It stands out that in Patient 3 half of the total volume is composed of the thrombus, which means it has grown significantly. Also in Patient 2, we find a big portion of the thrombus, while in Patient 1 the thrombus composes only 28.5% of the whole volume.
Looking at the literature, the role of tortuosity and asymmetry in AAA ruptures is not completely clear. Although we cannot conclude anything from their values, it is worth evaluating these indicators since they can be used as an additional diagnostic tool and predictors [21]-[22]. In the case of tortuosity, comparing the lumen and thrombus tortuosity could give additional information. In particular, the biggest difference is in Patient 3 which has $\tau_{thrombus} = 0.16$ and $\tau_{lumen} = 0.1$. This fact is confirmed by the asymmetry factor β, which is minimum in Patient 3, indicating the presence of an aneurysm that has developed in a preferred direction.
The last significant factor to consider is the time needed for the whole process. Manual segmentations take up to 40 minutes per patient, excluding the computation of the indicator, and have to be performed under the supervision of an expert surgeon. The automatic segmentation takes, on average, 7-8 minutes per patient, detecting all the structures and computing the indicators.

Finally, we show the centerlines of the patients and some orthogonal cutting of the surface. We recall that the orthogonal planes are taken with respect to the centerline.

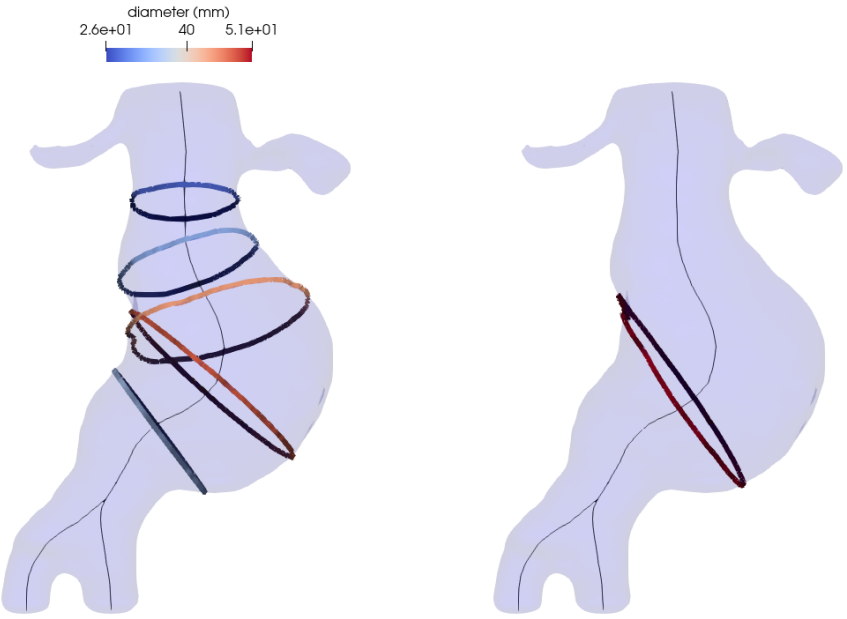

(a) Orthogonal cuttings (b) Biggest intersection

Figure 3.19: Centerlines and orthogonal intersections. (Patient 1)

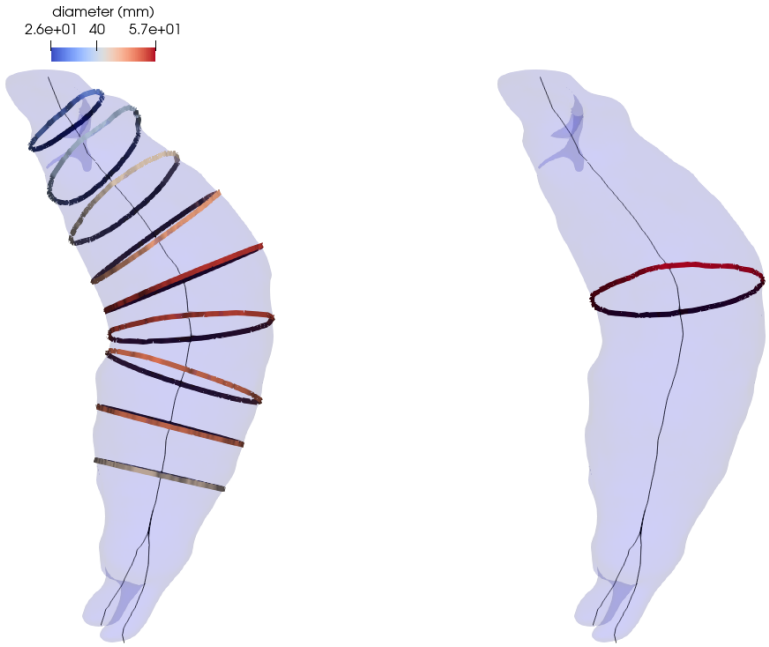

(a) Orthogonal cuttings (b) Biggest intersection

Figure 3.20: Centerlines and orthogonal intersections. (Patient 2)

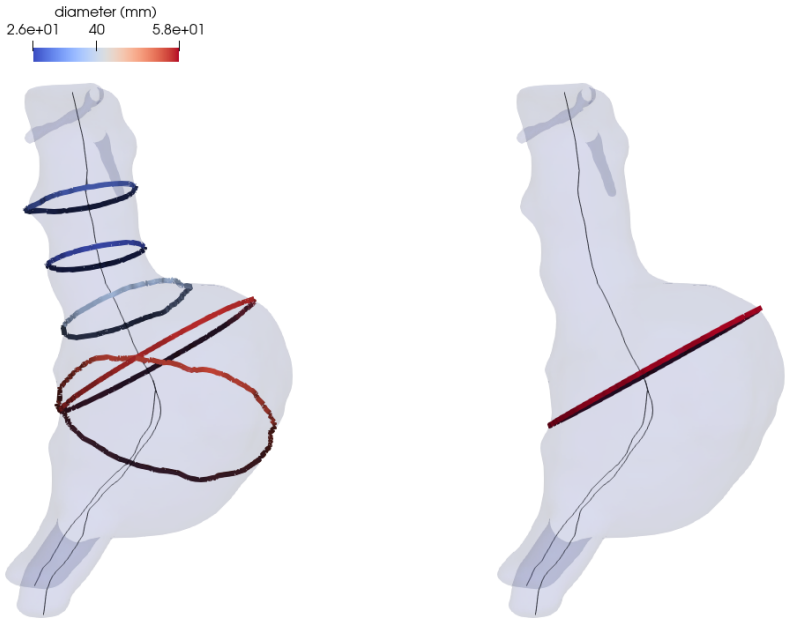

(a) Orthogonal cuttings (b) Biggest intersection

Figure 3.21: Centerlines and orthogonal intersections. (Patient 3)

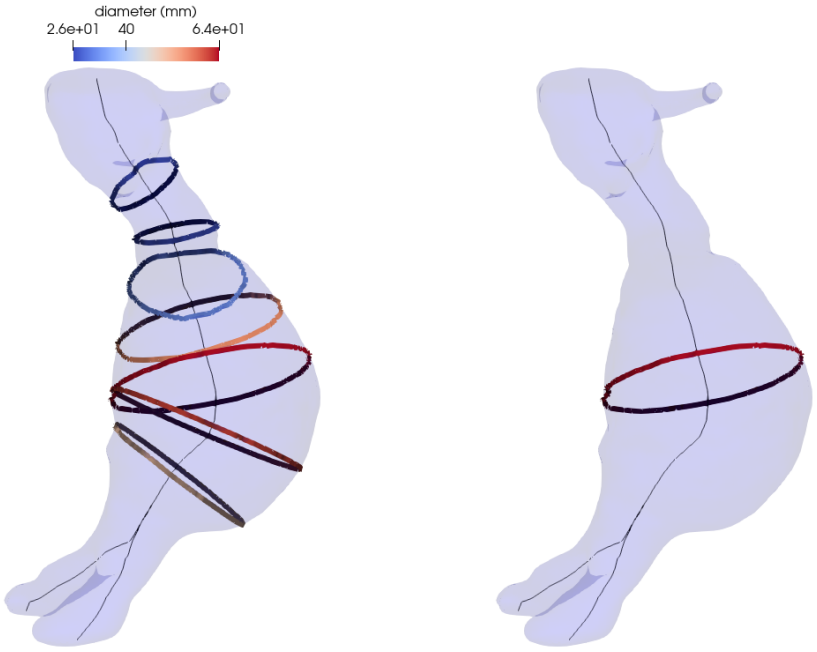

(a) Orthogonal cuttings (b) Biggest intersection

Figure 3.22: Centerlines and orthogonal intersections. (Patient 4)

4 | Conclusions and future developments

The thesis aimed to implement a fully automatic detection tool capable of identifying the aorta and the surrounding thrombus, in patients affected by abdominal aortic aneurysm, a vascular disease with a high mortality rate. This tool can have significant relevance in helping doctors with the diagnosis of the pathology and the pre-surgical planning.
We started by developing an algorithm to detect the lumen, based on its geometrical features and its high-intensity contrast in the CTAs scans. To guarantee that all the lumen was segmented, we also exploited the axial consistency, searching for intersections between the detection in adjacent slices. Then we refined the first detection guess, solving a minimization problem through morphological operators. The key idea of this approach is that differential operators, which compose PDEs (2.4) - (2.5), could be approximated by the successive application of morphological operators, such as *dilation* and *erosion* After obtaining a good estimate of the lumen, we moved to the more challenging part, the thrombus segmentation. To properly identify the thrombus, we split the segmentation into three steps. First, we made sure that the whole aneurysm was detected, we re-scaled the CTAs scans and we exploited, again, the morphological approach. Then we removed spurious extensions, using a 2D image convolution, and finally, we performed a last step of refinement. In the last part of the detection algorithm, we identified the calcifications around the aorta, and the aneurysm, since they could also be relevant to the doctors' decisions.
The 3D segmentations that we have obtained give an overview of how, and how big, the aneurysm develops, moreover they are easier to understand with respect to the CTAs scans. The doctors could need specific measures of the aneurysm, hence the qualitative results have to be coupled with quantitative measurements. To cope with that, we construct five different indicators which could support the doctors in their choices.
The algorithm shows good results both in terms of accuracy, and time with respect to the manual segmentation. The two more meaningful features of the detection tool are the automatization, in fact, manual inputs are not needed, and the robustness, which derives

from the fact that the parameters used in the algorithm are the same for all the patients.

In the future, the detection tool can be improved, using more advanced techniques, and extended towards different frameworks.
If we focus on the segmentation part, the two most crucial decisions are the choice of the filter and the selection of the segmentation technique. We decided to use a filter that, while smooths, tries to preserve the edges of the images. Even if it gives us satisfying results, compared to the other tested filters, we can perform broader research on that choice. Regarding the segmentation technique, we already saw in Chapter 1 that there is a variety of different algorithms exploited for medical purposes. Therefore, we can think of changing the method or, even better, combining different approaches trying to exploit their best features.
For what concern the indicators, we evaluate the measurements that, looking at the literature, we considered more relevant. This part can be extended in the future, by asking about the doctors' needs and implementing the latest useful indicators.
The final consideration on the implementation regards the available data. We develop the automatic detection tool by testing the algorithm on four patients only, and this is a limitation in many aspects. First of all, we have been able to analyze only a few numbers of CTAs, consequently, we have a restricted knowledge of anatomy and the aneurysm's features, and, more importantly, the assessment of the algorithm's robustness is not optimal. We should improve this aspect by looking at different CTAs, in order to see different behaviors in the aneurysm's development and generalize the code.
The quantity of CTAs is an interesting topic also for Deep Learning extension. As we can read in [11], there is the possibility of changing the approach completely and performing AAA detection through a Convolutional Neural Network. The usual problem with this type of method is that we need a large amount of CTAs, coupled with the AAA segmentation, to train the network. The automatic detection tool that we developed could partially help in this aspect. Indeed, to have a complete training set, an expert surgeon has to manually segment all the CTA in the dataset, then, only after this operation, it is possible to train the network. The automatic detection tool can substitute the expert and speed up the construction of the training set which will be used during the Deep Learning approach.

The detection tool can also be expanded to different fields. The development of the aneurysm could depend also on fluid dynamics quantities, hence we could introduce an additional step in the workflow.
After the automatic segmentation, we can exploit the 3D reconstructions by using them as

domains to asses fluid dynamics properties before and after surgery. The implementation of this ulterior step, together with the automatic segmentation, could give to doctors a complete analysis of the pathology and support the curative treatment of AAA.

Bibliography

[1] Shiping Zhu et al. "An Image Segmentation Algorithm in Image Processing Based on Threshold Segmentation". In: *2007 Third International IEEE Conference on Signal-Image Technologies and Internet-Based System*. Shanghai, China: IEEE, Dec. 2007, pp. 673–678. ISBN: 978-0-7695-3122-9. DOI: 10.1109/SITIS.2007.116.

[2] Javadpour A and Mohammadi A. "Improving Brain Magnetic Resonance Image (MRI) Segmentation via a Novel Algorithm based on Genetic and Regional Growth". eng. In: *Journal of Biomedical Physics & Engineering* 6.2 (June 2016), pp. 95–108. ISSN: 2251-7200.

[3] Asra Aslam, Ekram Khan, and M.M. Sufyan Beg. "Improved Edge Detection Algorithm for Brain Tumor Segmentation". en. In: *Procedia Computer Science* 58 (2015), pp. 430–437. ISSN: 18770509. DOI: 10.1016/j.procs.2015.08.057.

[4] E.A. Zanaty, Sultan Aljahdali, and Narayan Debnath. "A kernelized fuzzy c-means algorithm for automatic magnetic resonance image segmentation". In: *Journal of Computational Methods in Sciences and Engineering* 9.s2 (July 2009), S123–S136. ISSN: 18758983, 14727978. DOI: 10.3233/JCM-2009-0241.

[5] Pablo Marquez-Neila, Luis Baumela, and Luis Alvarez. "A Morphological Approach to Curvature-Based Evolution of Curves and Surfaces". In: *IEEE Transactions on Pattern Analysis and Machine Intelligence* 36.1 (Jan. 2014), pp. 2–17. ISSN: 0162-8828, 2160-9292. DOI: 10.1109/TPAMI.2013.106.

[6] Anthea Maton. *Human biology and health*. eng. 1st ed. OCLC: 32308337. Englewood Cliffs, N.J.: Prentice Hall, 1993. ISBN: 978-0-13-981176-0.

[7] Caren G Solomon and K Craig Kent. "Abdominal aortic aneurysms". In: *The New England Journal of Medicine* 371.22 (2014), p. 2101.

[8] Anders Wanhainen et al. "Editor's Choice – European Society for Vascular Surgery (ESVS) 2019 Clinical Practice Guidelines on the Management of Abdominal Aorto-iliac Artery Aneurysms". en. In: *European Journal of Vascular and Endovascular Surgery* 57.1 (Jan. 2019), pp. 8–93. ISSN: 10785884. DOI: 10.1016/j.ejvs.2018.09.020.

[9] George G Hartnell. "Imaging of aortic aneurysms and dissection: CT and MRI". In: *Journal of thoracic imaging* 16.1 (2001), pp. 35–46.

[10] Arthur W. Toga and John C. Mazziotta, eds. *Brain mapping: the methods*. 2nd ed. Amsterdam ; Boston: Academic Press, 2002. ISBN: 978-0-12-693019-1.

[11] Francesca Brutti et al. "Deep Learning to Automatically Segment and Analyze Abdominal Aortic Aneurysm from Computed Tomography Angiography". en. In: *Cardiovascular Engineering and Technology* (Jan. 2022). ISSN: 1869-408X, 1869-4098. DOI: 10.1007/s13239-021-00594-z.

[12] Fabien Lareyre et al. "A fully automated pipeline for mining abdominal aortic aneurysm using image segmentation". en. In: *Scientific Reports* 9.1 (Dec. 2019), p. 13750. ISSN: 2045-2322. DOI: 10.1038/s41598-019-50251-8.

[13] Pietro Perona and Jitendra Malik. "Scale-space and edge detection using anisotropic diffusion". In: *IEEE Transactions on pattern analysis and machine intelligence* 12.7 (1990), pp. 629–639.

[14] Ross T Whitaker and Xinwei Xue. "Variable-conductance, level-set curvature for image denoising". In: *Proceedings 2001 International Conference on Image Processing (Cat. No. 01CH37205)*. Vol. 3. IEEE. 2001, pp. 142–145.

[15] Satoshi Suzuki et al. "Topological structural analysis of digitized binary images by border following". In: *Computer vision, graphics, and image processing* 30.1 (1985), pp. 32–46.

[16] Stanley Osher and James A Sethian. "Fronts propagating with curvature-dependent speed: Algorithms based on Hamilton-Jacobi formulations". en. In: *Journal of Computational Physics* 79.1 (Nov. 1988), pp. 12–49. ISSN: 00219991. DOI: 10.1016/0021-9991(88)90002-2.

[17] Luis Alvarez et al. "Axioms and fundamental equations of image processing". en. In: *Archive for Rational Mechanics and Analysis* 123.3 (1993), pp. 199–257. ISSN: 0003-9527, 1432-0673. DOI: 10.1007/BF00375127.

[18] T.F. Chan and L.A. Vese. "Active contours without edges". In: *IEEE Transactions on Image Processing* 10.2 (Feb. 2001), pp. 266–277. ISSN: 10577149. DOI: 10.1109/83.902291.

[19] Jesús Urrutia et al. "Geometric surrogates of abdominal aortic aneurysm wall mechanics". eng. In: *Medical Engineering & Physics* 59 (Sept. 2018), pp. 43–49. ISSN: 1873-4030. DOI: 10.1016/j.medengphy.2018.06.007.

[20] Luca Antiga. "Patient-Specific Modeling of Geometry and Blood Flow in Large Arteries". URL: https://lantiga.github.io/media/AntigaPhDThesis.pdf.

[21] Barry J. Doyle et al. "Vessel asymmetry as an additional diagnostic tool in the assessment of abdominal aortic aneurysms". In: *Journal of Vascular Surgery* 49.2

(2009), pp. 443–454. ISSN: 0741-5214. DOI: https://doi.org/10.1016/j.jvs.2008.08.064.

[22] Sally H Choi et al. "Evaluation of Aortic Tortuosity as a Negative Predictor of Abdominal Aortic Aneurysm Rupture". In: *Journal of Vascular Surgery* 74.3 (2021), e102.

[23] Lukas Radl et al. "AVT: Multicenter aortic vessel tree CTA dataset collection with ground truth segmentation masks". en. In: *Data in Brief* 40 (Feb. 2022), p. 107801. ISSN: 23523409. DOI: 10.1016/j.dib.2022.107801.

[24] Song Yuheng and Yan Hao. "Image segmentation algorithms overview". In: *arXiv preprint arXiv:1707.02051* (2017).

[25] Jonathan Sachs. "Digital image basics". In: *Digital Light & Color* 1996 (1999).

List of Figures

List of Tables

Acknowledgements

Il primo ringraziamento va al professor Luca Formaggia che si è preso l'incarico di farmi da relatore per questa tesi, e che col suo corso di C++ mi ha mostrato veramente cos'è la programmazione. Desidero ringraziare quindi i miei correlatori Abele e Luca, che mi hanno supportato durante l'intero sviluppo della tesi, risolvendo sempre efficacemente ogni mio dubbio o problema.

Poi arrivano i ringraziamenti a mamma e papino. Siete stati e sarete i miei modelli, quando penso al futuro il mio più grande obiettivo è crescere e diventare come voi. Sono riuscito a finire questo percorso grazie al vostro affetto che mi ha supportato continuamente, ogni istante. Ringrazio anche Dada che, nonostante sia sempre in giro per il mondo, c'è sempre quando ho bisogno ed è una delle persone che stimo di più per quello che fa e per la sua intraprendenza.

Un grosso ringraziamento a Roberto, che dopo i miei genitori è la persona che vedo più spesso, tutte le volte che ci vediamo la risata è assicurata, potremmo essere chiusi in una stanza e continuerremo a ridere all'infinito per le stesse battute che facciamo da 12 anni. Inoltre, è l'unica persona che non ho mai visto arrabiata. Un altro grosso ringraziamento a quel matto di Nicco per le sue riflessioni filosofiche e perchè, pur conoscendolo da una vita, non riesco ancora a capire quando è serio e quando mi sta prendendo in giro. Un ringraziamento di cuore anche alle mie amiche di sempre. Costanza, la migliore amica con cui fare versi e strette di mano originali. Chiara, la migliore amica se vuoi qualcuno che ti inciti (fino alla disperazione) per trovare il parcheggio vicino al bar o ristorante. Camilla, apparentemente ci odiamo ma in realtà ci vogliamo bene. Sofia, grazie per tutte le passeggiate passate a risolvere i mie problemi. Elisa, prima conosciuta come "la sorella di Roberto" ma poi diventata vera amica. Emilia, la migliore influencer dell'Impruneta. Un ringraziamento speciale a Viola che si è sorbita qualsiasi mio stato d'animo, ma nonostante ciò mi è sempre rimasta vicina.

Ringrazio i miei più cari amici del liceo Vanno, Cosimo, Sho, Matteo e Allegra. Non ci vediamo molto spesso ma quando ci vediamo è sempre una festa, ed è come tornare ai bei vecchi tempi della 5B.

Come non ringraziare i miei colleghi dell'università. Giulia (Mesc) grazie per le innumerevoli consultazioni pre e post esame, penso veramente che senza la tua amicizia e supporto il mio percorso sarebbe andato diversamente (peggio). Eleonora grazie per far sembrare le pause pranzo infinite con le tua velocità nel finire la schiscetta. Filippo grazie per essere sempre l'anima della festa. Luca grazie di lamentarti di continuo, così da rendermi più ottimista. Sara grazie per riuscire a fare tutto con grande nonchalance.

Un takksigelse ai miei amici dell'erasmus Isa, Fra, Fra Fit e VeronicaDaBrescia. Ero partito per l'erasmus con il morale sotto ai piedi, voi avete trasformato quei 4 mesi e mezzo in uno dei periodi più belli della mia vita. Ricorderò per sempre le nostre cene da 1000 NOK, la pizza di Una, la pentola del tè usata per altri scopi e tutte le altre avventure che abbiamo passato insieme.

L'ultimo ringraziamento è per la persona che più mi è stata vicina. La persona che ha gioito con me quando le cose andavano bene, ma che soprattuto mi ha sempre tranquillizzato e sostenuto quando le cose andavano male. La persone con cui ho riso, e con cui ho pianto. La persona a cui ho dato tanto ma non abbastanza. La persona che, a prescindere da qualsiasi cosa, rimarrà per sempre la più speciale cha abbia conosciuto. Per questi e altri n motivi, dedico la tesi a Giulia.